

This discussion paper is/has been under review for the journal Atmospheric Chemistry and Physics (ACP). Please refer to the corresponding final paper in ACP if available.

Hindcast experiments of tropospheric composition during the summer 2010 fires over Western Russia

V. Huijnen¹, J. Flemming², J. W. Kaiser², A. Inness², J. Leitão³, A. Heil⁴,
H. J. Eskes¹, M. G. Schultz⁴, A. Benedetti², G. Dufour⁵, and M. Eremenko⁵

¹Royal Netherlands Meteorological Institute, De Bilt, The Netherlands

²European Centre for Medium-Range Weather Forecasts (ECMWF), Reading, UK

³Institute of Environmental Physics, University of Bremen, Bremen, Germany

⁴Forschungszentrum Jülich, Jülich, Germany

⁵Laboratoire Inter-universitaire des Systèmes Atmosphériques (LISA), UMR7583, CNRS/INSU – Universités Paris Est Créteil et Paris Diderot, Créteil, France

Received: 10 November 2011 – Accepted: 15 November 2011 – Published: 5 December 2011

Correspondence to: V. Huijnen (huijnen@knmi.nl)

Published by Copernicus Publications on behalf of the European Geosciences Union.

Hindcast experiments of tropospheric composition

V. Huijnen et al.

Title Page

Abstract

Introduction

Conclusions

References

Tables

Figures

⏪

⏩

◀

▶

Back

Close

Full Screen / Esc

Printer-friendly Version

Interactive Discussion

Abstract

The severe wildfires in Western Russia during July–August 2010 coincided with a strong heat wave and led to large emissions of aerosols and trace gases such as carbon monoxide (CO), hydrocarbons and nitrogen oxides into the troposphere.

This extreme event is used to evaluate the ability of the global MACC (Monitoring Atmospheric Composition and Climate) atmospheric composition forecasting system to analyze large-scale pollution episodes and to test the respective influence of a priori emission information and data assimilation on the results. Daily 4-day hindcasts were conducted using assimilated aerosol optical depth (AOD), CO, nitrogen dioxide (NO₂) and ozone (O₃) data from a range of satellite instruments. Daily fire emissions were used from the Global Fire Assimilation System (GFAS) version 1.0, derived from satellite fire radiative power retrievals.

The impact of accurate wildfire emissions is dominant on the composition in the boundary layer, whereas the assimilation system influences concentrations throughout the troposphere, reflecting the vertical sensitivity of the satellite instruments. The application of the daily fire emissions reduces the area-average mean bias by 63 % (for CO), 38 % (O₃) and 64 % (NO₂) during the first 24 h, compared to a reference simulation with a multi-annual mean climatology of biomass burning emissions. When initial tracer concentrations are further constrained by data assimilation, biases are reduced by 87, 38 and 80 %. The forecast accuracy, quantified by the mean bias up to 96 h lead time, was best for all compounds when using both the GFAS emissions and assimilation. The model simulations suggest an indirect positive impact of O₃ and CO assimilation on hindcasts of NO₂ via changes in the oxidizing capacity.

However, the quality of local hindcasts was strongly depending on the assumptions made for forecasted fire emissions. This was well visible from a relatively rapid increase by the root mean square error with respect to ground-based data for AOD, and satellite based NO₂. This calls for a more advanced method to forecast fire emissions than the currently adopted persistency approach.

Hindcast experiments of tropospheric composition

V. Huijnen et al.

Title Page

Abstract

Introduction

Conclusions

References

Tables

Figures

⏪

⏩

◀

▶

Back

Close

Full Screen / Esc

Printer-friendly Version

Interactive Discussion



The combined analysis of fire radiative power observations, multiple trace gas and aerosol satellite observations, as provided by the MACC system, results in a detailed quantitative description of the impact of major fires on atmospheric composition, and demonstrate the capabilities for the real-time analysis and forecasts of large-scale fire events.

1 Introduction

In summer 2010, Western Russia experienced a long atmospheric blocking period (Matsueda, 2011; Dole et al., 2011) resulting in a strong heat wave, which started around 27 June and lasted until 14 August. Within a region of $1000 \times 1000 \text{ km}^2$ around Moscow, temperatures were approximately $5\text{--}10^\circ\text{C}$ warmer and relative humidity was 20–40 % lower than normal (Dole et al., 2011; Witte et al., 2011). The combination of high temperatures and drought made the vegetation vulnerable to fires, including the peat soil deposits that are common in this region. The Moderate Resolution Imaging Spectroradiometer (MODIS) instrument observed increased intensities of fire radiative power (FRP) over Western Russia from 20 July onwards, and these fires resulted in periods of high pollution levels in Moscow and its vicinity. The combination of hot temperatures and pollutants emitted from the fires was estimated to have led to a significant increase in deaths in Moscow (van Donkelaar et al., 2011).

A range of observations were used in various studies to characterize the tropospheric composition during this episode, including in-situ data for fine and coarse aerosol mass ($\text{PM}_{2.5}$ and PM_{10} , van Donkelaar et al., 2011), ozone (O_3) and carbon monoxide (CO) (Konovalov et al., 2011), CO total columns (Yurganov et al., 2011), as well as space-based information of CO total columns from Atmospheric Infrared Sounder (AIRS), and aerosol optical depth (AOD) and single-scattering albedo from Ozone Monitoring Instrument (OMI) (Witte et al., 2011). In addition, it had been shown before that fire episodes can be analyzed by the Infrared Atmospheric Sounding Interferometer (IASI) CO (Turquety et al., 2009) as well as nitrogen dioxide (NO_2) and formaldehyde (HCHO)

Hindcast experiments of tropospheric composition

V. Huijnen et al.

Title Page

Abstract

Introduction

Conclusions

References

Tables

Figures



Back

Close

Full Screen / Esc

Printer-friendly Version

Interactive Discussion



observations from the OMI and Scanning Imaging Absorption SpectroMeter for Atmospheric ChartographY (SCIAMACHY) instruments (e.g., Mebust et al., 2011; Stavrou et al., 2009).

The pollution levels by aerosol, CO and O₃ in Moscow varied greatly during the period, both due to changing wind directions, and due to variations in fire emissions. Meteorological conditions during a heat wave are well known to affect tropospheric composition (Ordóñez et al., 2010). Changes in land surface parameters can alter dry deposition over vegetation (Vautard et al., 2005), and biogenic emissions (Lee et al., 2006; Solberg et al., 2008). Apart from these direct effects, trace gas concentrations vary due to perturbations of the chemical production and loss rates (e.g., Duncan et al., 2003). Additionally, depending on the optical properties of emitted aerosol, O₃ and NO₂ photolysis rates can be reduced (Real et al., 2007). All these factors demand a comprehensive modeling framework in order to produce a realistic analysis and forecast of all aspects influencing tropospheric composition. This includes the use of data assimilation of meteorology and chemical composition, as well as accurate time- and space resolved near real-time (NRT) emission estimates (Hodzic et al., 2007; Menut and Bessagnet, 2010).

In the MACC (Monitoring Atmospheric Composition and Climate, <http://www.gmes-atmosphere.eu>) project, analyses and forecasts of atmospheric composition are routinely produced based on the coupled system CTM-IFS (Chemistry Transport Model – Integrated Forecast System, Flemming et al., 2009), extended with an aerosol model within the IFS (Morcrette et al., 2009; Benedetti et al., 2009). This data assimilation system makes use of analyses of both meteorology and chemical composition (Hollingsworth et al., 2008). Thus, it is able to monitor variations in chemical composition due to varying meteorology, such as episodes of increased ozone levels caused by heat waves (Ordóñez et al., 2010), or the onset of the ozone hole (Flemming et al., 2011). Elguindi et al. (2010) showed that the assimilation of MOPITT-CO total column data largely helped to reduce model biases in background concentrations. They also showed that accurate emission estimates are needed for modeling the long-range

Hindcast experiments of tropospheric composition

V. Huijnen et al.

[Title Page](#)[Abstract](#)[Introduction](#)[Conclusions](#)[References](#)[Tables](#)[Figures](#)[⏪](#)[⏩](#)[◀](#)[▶](#)[Back](#)[Close](#)[Full Screen / Esc](#)[Printer-friendly Version](#)[Interactive Discussion](#)

transport of pollutants. Within MACC, a NRT daily fire emission estimate based on FRP observations from MODIS was developed: the Global Fire Assimilation System (GFAS, Kaiser et al., 2011).

The summer 2010 wildfires over Western Russia provide an opportunity for a comprehensive assessment of the MACC assimilation/forecast system for this type of extreme pollution event. In this paper, we focus on the following questions: how does the free running forecast system using the GFAS emissions perform compared to ground-based and satellite observations? What is the relative importance of the chemical assimilation and, on the other hand, the fire emission estimates for the tropospheric distribution of the fields, both for the analyses and the hindcasts issued from them? Considering the chemical interaction within the system, how do assimilation and the GFAS emissions influence the model chemical composition, e.g. by changes in the oxidative capacity? These questions may help to identify causes of variations in forecast accuracy from the perspective of both the modeling and the observing framework and can provide guidelines for future developments.

The paper is structured as follows: We describe the assimilation and forecast framework, together with the GFAS system in Sect. 2. In Sect. 3 various hindcast experiments are evaluated against independent observations for the heat wave period in Western Russia. The interactions of the different modeling components with each other are explicitly discussed in Sect. 4. We end this paper with a summary and conclusions from the analysis performed.

2 The MACC system and experiment setup

2.1 The global assimilation and forecast system

The MACC system (Hollingsworth et al., 2008) is used to perform assimilation and hindcast experiments of the chemical composition of the troposphere and stratosphere on a global scale. Daily analyses and forecasts of greenhouse gases, reactive

Hindcast experiments of tropospheric composition

V. Huijnen et al.

Title Page

Abstract

Introduction

Conclusions

References

Tables

Figures



Back

Close

Full Screen / Esc

Printer-friendly Version

Interactive Discussion



gases and aerosols, as well as a comprehensive reanalysis of atmospheric composition data over the period 2003–2010 are available via the MACC project web-portal (<http://www.gmes-atmosphere.eu/data/>). Aerosols are modeled within the IFS (Morcrette et al., 2009). The chemistry of reactive gases is calculated by a separate chemistry transport model. For this study we use the TM5 model (Huijnen et al., 2010a), which is coupled to the IFS via the OASIS4 coupler (Redler et al., 2009), as described in Flemming et al. (2009). At the moment no interaction between aerosols and trace gas concentrations is considered.

The ECMWF 4D-Var meteorological assimilation system has been extended to assimilate chemically reactive trace gas concentrations and AOD from satellite retrievals (Inness et al., 2009; Benedetti et al., 2009). In the daily analyses for 2010, 7 retrieval products from 7 satellite instruments were routinely assimilated, see Table 1. The observational data are thinned to $1^\circ \times 1^\circ$ resolution. Variational quality control (Andersson and Järvinen, 1999) and first guess checks are switched off for CO and NO₂, to avoid that observations with high values that are very different from the background values would be given only little weight in the analysis or even be rejected. As an example, the mean averaging kernel for the IASI CO product over Western Russia, between 20 July and 15 August, is given in Fig. 1. It shows that the instrument is sensitive down to the surface (for daytime observations), but the largest sensitivity to CO is at an altitude of approx. 400 hPa. By constraining both the ozone total column, using SCIAMACHY, OMI and SBUV, and the partial ozone column in the stratosphere, using MLS data, tropospheric O₃ is directly affected by the assimilation procedure (Flemming et al., 2011). The 4D-Var system runs on T159L60 resolution, and minimizes the difference between the observation and the background fields during a 12 h assimilation window.

The hindcast experiments use meteorology initialized by the ECMWF operational analyses. For the analysis of chemical composition the assimilation window is 12 h, starting at 21 and 9 UTC. Every day at 0 UTC a 4-day (96 h) hindcast is started with the same system. The hindcasts use either the optimized initial concentration fields based on the data assimilation system, or the first day hindcasts for aerosol, O₃, CO and NO_x

Hindcast experiments of tropospheric composition

V. Huijnen et al.

Title Page

Abstract

Introduction

Conclusions

References

Tables

Figures



Back

Close

Full Screen / Esc

Printer-friendly Version

Interactive Discussion



(= NO + NO₂) of the previous day for the reference hindcast runs. The four hindcast days are referred to as D + 0 to D + 3.

The TM5 model uses the tropospheric gas-phase chemistry version TM5-chem-v3.0 (Huijnen et al., 2010a), which is based on CBM-IV chemistry. It applies the same 60 level vertical discretization as the IFS, but the horizontal resolution is 3° lon × 2° lat, globally. The standard biomass burning emissions in the TM5 reference hindcast experiments are based on GFEDv2 (van der Werf et al., 2006) monthly mean “climato-logical” emissions calculated from the years 2001–2006. The injection height of the reactive gases is assumed to extend up to 2 km (distributed as 20 % in layers 0–100 m, 100–500 m and 500–1000 m, respectively, and 40 % in 1000–2000 m), in line with the study from Val Martin et al. (2010).

2.2 The GFAS emissions

Numerous systems for the derivation of fire emission estimates have been developed. They are traditionally based on burned area, e.g., Andreae and Merlet (2001), van der Werf et al. (2006, 2010), Wiedinmyer et al. (2010). Several recent developments have instead used Fire Radiative Power (FRP) observations, e.g., Kaiser et al. (2009), Sofiev et al. (2009), Konovalov et al., (2011), because FRP has been shown to be directly proportional to the combustion and aerosol emission rates (Wooster et al., 2005; Ichoku and Kaufman, 2005; Heil et al., 2010). Common sources of uncertainty for all approaches are the land cover (and corresponding fire) type as well as the corresponding emission factors (Andreae and Merlet, 2001; Wiedinmeyr et al., 2010; van der Werf et al., 2010; Mebust et al., 2011; Akagi et al., 2011). In the MACC project a NRT Global Fire Assimilation System (GFAS) was developed to estimate daily fire emission rates. The latest version (GFASv1.0), described in Kaiser et al. (2011), is based on FRP observations derived from the MODIS satellite instruments, and provides emission estimates on a daily basis with global coverage on a 0.5° × 0.5° spatial grid.

Hindcast experiments of tropospheric composition

V. Huijnen et al.

Title Page

Abstract

Introduction

Conclusions

References

Tables

Figures



Back

Close

Full Screen / Esc

Printer-friendly Version

Interactive Discussion



The amount of trace gases released from the fires strongly depends on the predominant land cover type classification. The emission rate f_s for species s is calculated as:

$$f_s = \rho \alpha \beta_s \quad (1)$$

where α denotes a biome-dependent factor for the conversion of FRP observations ρ to the rate of dry matter burned and β_s are the biome-dependent emission factors from Andreae and Merlet (2001) with updates, which are of similar magnitude as those specified for GFEDv3.1 (van der Werf et al., 2010). In GFASv1.0 the conversion factor α was derived with a linear regression between the observed fire radiative energy and the dry matter burned in the GFEDv3.1 inventory. Specific conversion factors have been derived for eight dominant fire type classes (Heil et al., 2010; Kaiser et al., 2011). The dominant fire type map was derived from the historic distribution of fire types in GFEDv3.1. For Russia, peat (histosols) and peaty soil areas were added using information from Stolbovoi and Savin (2002) and (FAO 2003). GFASv1.0 is consistent with GFED3.1 within its accuracy limits and captures many small fires that are missing in the GFEDv3.1 inventory. For aerosol emissions a global enhancement factor of 3.4 is introduced to compensate the under-estimation of bottom-up compared to top-down fire emissions at a regional to global scale (Kaiser et al., 2011). With this correction factor, the GFASv1.0 aerosol emissions of the Western Russian fires of 2010 are consistent with Eastern European AERONET observations (Kaiser et al., 2011).

The GFASv1.0 emissions for aerosols and all relevant reactive trace gases, including the non-methane volatile organic carbons (NMVOC's), are applied to the MACC system globally. A constant emission rate during the day is applied, which is a reasonable assumption for this case study where nighttime fire activity almost equaled daytime burning (Kaiser et al., 2011). The D + 0 fire emissions are assumed to be constant during the full hindcast period.

Hindcast experiments of tropospheric composition

V. Huijnen et al.

[Title Page](#)[Abstract](#)[Introduction](#)[Conclusions](#)[References](#)[Tables](#)[Figures](#)[⏪](#)[⏩](#)[◀](#)[▶](#)[Back](#)[Close](#)[Full Screen / Esc](#)[Printer-friendly Version](#)[Interactive Discussion](#)

2.3 Set-up of the model experiments

To investigate the impact of both the assimilation system and the fire emissions, we performed four different 4-day hindcast runs, namely with and without initializing aerosol, CO, O₃ and NO_x from assimilated fields, and using either the GFASv1.0 fire product or the GFEDv2 climatological emissions, see Table 2. All runs lasted up to 31 August, while the free runs started on 1 July, and the runs including assimilation on 15 July. In this study we will primarily focus on the evaluation of trace gas concentrations in the free troposphere, on a sub-continental scale (~ 1000 × 1000 km), having in mind the relatively coarse resolution of our chemistry model.

3 Results

3.1 Meteorology and fire emissions

Figure 2 illustrates the meteorological situation for the July–August time period over Western Russia, here defined as the region 35° E–70° E, 45° N–65° N (see also Fig. 3). The heat wave started around 27 June and lasted until 14 August. Temperatures reached maximum values of 39°C, at the end of July, at individual locations (Matsueda, 2011), and were on average 5–10°C higher than normal (Dole et al., 2011). No significant precipitation was recorded during this period, which resulted in relative humidity levels 20–40% lower than normal (Witte et al., 2011). According to the meteorological analyses, from mid-July onwards the soil wetness was below the critical level of 23%, where water stress in vegetation occurs. From this period onwards the FRP of GFASv1.0 starts to increase, with extreme magnitudes on 29–30 August. On the evening of 10 August thunderstorms cleared the air over Moscow. After this date the recorded number of fires, and hence the fire emissions, were reduced. On 13 August the heat wave ended with heavy rain in Moscow and nearby areas.

Hindcast experiments of tropospheric composition

V. Huijnen et al.

Title Page

Abstract

Introduction

Conclusions

References

Tables

Figures

⏪

⏩

◀

▶

Back

Close

Full Screen / Esc

Printer-friendly Version

Interactive Discussion



using assimilated surface CO concentrations. Their estimated contribution from peat fires was $\sim 30\%$.

During 29 and 30 July, the release of CO in GFASv1.0 is estimated as $\sim 3.6\text{ Tg}$, contributing more than 30% of the total wildfire emissions over Western Russia during July and August 2010. Fire emissions for NO_x have almost doubled compared to the climatology and contribute 32% to the total emissions during this period.

3.2 Evaluation of tropospheric composition

The hindcast experiments (see Table 2) have been compared against various observations that were not used in the assimilation, as will be described in the corresponding subsections. For modeled AOD, ground-based observations done at the Moscow AERONET station (37.5° E , 55.7° N) are used. In the case of CO, O_3 , NO_2 and HCHO, retrievals from MOPITT, IASI and SCIAMACHY are used.

Forecast accuracy is quantified in terms of mean bias and Root Mean Square Error (RMSE), which have been calculated on a daily basis for each hindcast day and model grid-box. These were then averaged over the Western Russia region and for the time frame of 20 July–15 August. For the AOD hindcasts, error measures are computed based on bias and RMSE with respect to the Moscow station only. Model AOD is interpolated to the time of the individual observations, and equal weight is given to all separate days in the time series.

3.2.1 Aerosol optical depth and aerosol composition

In Fig. 4, the modeled total AOD at 550 nm from the four configurations is compared to AERONET observations at the Moscow station. Prior to the fire event (15–25 July) all model configurations tend to underestimate the AOD, although the configurations including initialization from assimilated AOD provide the best results. During the fire period, the run Assim captures a substantial part of the individual events, but frequently underestimates the magnitudes of the AODs. The run GFAS performs better, capturing

Hindcast experiments of tropospheric composition

V. Huijnen et al.

Title Page

Abstract

Introduction

Conclusions

References

Tables

Figures

⏪

⏩

◀

▶

Back

Close

Full Screen / Esc

Printer-friendly Version

Interactive Discussion



most of the individual events. For instance, on 7 August, the very high levels of modeled AOD are in agreement with a observed daily mean AOD, with a value of 3.3 in GFAS compared to 3.6 in the observations.

Despite the similarity in AOD in the assimilation runs with/without GFASv1.0, the aerosol composition in these runs is very different, see Fig. 4. In the assimilation runs excluding GFASv1.0 emissions the increase in AOD is largely attributed to sulphate, dust and sea salt aerosols. In the other runs the organic matter and black carbon aerosols, which are the dominant aerosol types in smoke, are most enhanced. Therefore, realistic fire smoke emissions are essential for the ability to identify elevated aerosol levels as smoke. This behavior is expected as the aerosol assimilation scheme does not contain information of the aerosol composition but it relies on a realistic first guess estimation of emission (Benedetti et al., 2009).

The mean bias for run GFAS on D + 0 is improved by 88 % compared to run CNT and by 75 % compared to run Assim, see Table 4. It remains better than for runs CNT and Assim throughout the hindcast period. This shows that the GFAS aerosol emissions also yield information on the total aerosol load that is more accurate than a climatology and even the MODIS AOD observations in this particular case. However, the information of GFAS and MODIS AOD is complementary and the mean bias of run Assim-GFAS is consequently the lowest of all runs up to D + 2. The two runs with GFAS emissions show an increase in mean bias for D + 3. We interpret this as a symptom of a false alarm due to the assumption of persistence of the emissions from D + 0, in particular persistence of the extreme emission rates on 29–30 July. This false alarm is visible around 3 August in the AOD time series for D + 3 in the top right panel of Fig. 12 in Kaiser et al. (2011).

The RMSE for run GFAS shows the positive impact of the GFAS emissions up to D + 3 compared to run CNT. Run Assim-GFAS is better than the runs GFAS and Assim up to D + 2, once again showing the complementary positive impacts of the assimilation and the emissions. The RMSE for D + 3 in run Assim-GFAS is slightly worse than the one in run Assim. This is a consequence of the strong sensitivity of this error metric

Hindcast experiments of tropospheric composition

V. Huijnen et al.

[Title Page](#)[Abstract](#)[Introduction](#)[Conclusions](#)[References](#)[Tables](#)[Figures](#)[Back](#)[Close](#)[Full Screen / Esc](#)[Printer-friendly Version](#)[Interactive Discussion](#)

to the actual variability in the emissions, which was very large between 28 July and 14 August. The RMSE is negatively affected by the emission persistency assumption made within each hindcast. A detailed interpretation is, however, beyond the scope of the present study because RMSE also becomes sensitive to the activity of the forecast at longer lead times.

In summary, the composition of the smoke aerosol plume is only realistic when GFAS emissions are used, the mean bias of AOD are improved by using the GFAS emissions throughout the AOD forecasts and the RMSE up to D + 2. The RMSE illustrates that the day-to-day variability in the emissions, and also AOD at the individual sites, are very high.

3.2.2 Carbon monoxide

For the evaluation of CO, daytime total column observations from the MOPITT-V4 product (Deeter et al., 2010) have been used. We apply the MOPITT averaging kernels to the logarithm of the modeled profile. The average total CO columns over Western Russia for run GFAS during the time of the fires shows a strong improvement compared to the control run. A similar pattern as that from MOPITT can be observed, although with an overall negative bias (Fig. 5). A better agreement is found with run Assim-GFAS, which, on average, captured the observed magnitude well. The impacted region spans an area from the western border of Russia, 35° E, up to 80° E and from 40° N to 65° N, as a consequence of the relatively long CO lifetime.

The evolution of the area-average total columns over Western Russia is presented in Fig. 6. Run GFAS accurately follows the observed area-average increase and decrease, but with a fairly constant negative offset during the whole simulation period. This suggests that the bias is not directly related to the GFAS CO emissions but rather to a general bias in CO over the Northern Hemisphere, see also Huijnen et al. (2010a).

When using assimilated IASI CO observations for the hindcast initialization, the average model total columns are low by $\sim 10^{17}$ molec cm⁻² ($\sim 6\%$) compared to MOPITT-V4 during the initial phase, i.e., before 3 August. This bias is of the same magnitude

Hindcast experiments of tropospheric composition

V. Huijnen et al.

Title Page

Abstract

Introduction

Conclusions

References

Tables

Figures

⏪

⏩

◀

▶

Back

Close

Full Screen / Esc

Printer-friendly Version

Interactive Discussion



**Hindcast
experiments of
tropospheric
composition**

V. Huijnen et al.

Title Page

Abstract

Introduction

Conclusions

References

Tables

Figures

⏪

⏩

◀

▶

Back

Close

Full Screen / Esc

Printer-friendly Version

Interactive Discussion

as for the average over the extra-tropical Northern Hemisphere (30° N–90° N). However, during the period of the highest CO columns (4–14 August), a positive bias of up to $0.5 \times 10^{18} \text{ molec cm}^{-2}$ was found. These differences could be related to differences between IASI and MOPITT CO retrieval algorithms during this particular case, as discussed in Turquety et al. (2009) and George et al. (2009). The assimilation runs with and without GFAS emissions do not show a significant difference for D + 0 hindcasts, illustrating the dominating impact of the initialization by assimilation of IASI observations.

A quantitative analysis of the forecast error as function of the hindcast day is given in Table 5. For the D + 0 hindcasts the mean bias in run GFAS is $-0.29 \times 10^{18} \text{ molec cm}^{-2}$. This remains fairly constant for the next three hindcast days and is less than half the bias obtained for run CNT.

It is interesting to consider the differences in the evolution of bias and RMSE at increasing forecast lengths between runs Assim and Assim-GFAS. Initially, for D + 0, these numbers are similar, but while in run Assim a negative bias develops quickly, this happens to a lesser extent in run Assim-GFAS, with an improvement of the mean bias relative to run Assim of 84 % at D + 3. This demonstrates that the total amount of CO emissions, which is for this event much lower in run Assim (climatological) than in Assim-GFAS (persistence of D + 0 emissions), is important to obtain a good forecast accuracy.

On the other hand, the values for RMSE increase considerably when including the GFAS emissions. This reflects the poor forecast accuracy of the precise emission pattern based on the persistence assumption in the fire emissions, as found before in the AOD analysis.

Figure 7 shows a time evolution of the daily maximum CO concentrations averaged over Western Russia. The area-averaged values obtained for the model configurations that include the GFAS emissions are as high as $\sim 500 \text{ ppbv}$, which is about 5 times the normal concentration, given by the CNT run. Note that locally the CO concentrations have reached much larger values. In run Assim the surface CO concentrations

are increased by $\sim 33\%$, despite the fact that largest background errors for CO are specified at the lowest altitude levels (Inness et al., 2009). This can be explained by the low sensitivity of IASI near the surface, as illustrated by the averaging kernel in Fig. 1, and because the a-priori profiles do not contain the high surface concentrations for this particular event. The average surface CO concentrations in run Assim-GFAS are $\sim 55\%$ larger compared to run Assim. When analyzing the area-average vertical model profiles (Fig. 8), the impact of the CO assimilation in run Assim is visible throughout the full troposphere, up to 200 hPa, with the largest increase in CO concentrations at around 700 hPa. In contrast, the runs with GFAS show high CO concentrations up to ~ 800 hPa, corresponding to the injection height distribution of the CO emissions. Switching on the assimilation in run Assim-GFAS results in a marginal increase of the high concentrations in the boundary layer, but shows a more effective increase between 800 and 400 hPa. This explains the removal of the negative bias with respect to MOPITT.

3.2.3 Tropospheric ozone

We use IASI O_3 partial tropospheric columns (0–6 km) from LISA (Dufour et al., 2011) to evaluate hindcasts of tropospheric O_3 concentrations. The O_3 data consist of a profile retrieval using the radiative transfer model KOPRA (Karlsruhe Optimised and Precise Radiative transfer Algorithm, Stiller et al., 2000) and its inversion module KOPRAFIT (Eremenko et al., 2008). Note that the IASI observations are filtered for cloud contamination before the retrieval. This filter should allow also screening for the worst aerosol contaminated pixels. However, the retrieval algorithm does not account for aerosol concentrations, and moderate aerosol loading can potentially introduce significant biases in the ozone retrieval depending on the type, size, altitude and amount of aerosols. The product used here was available for Europe and Western Russia up to 58° E. In the validation procedure we map spatially and temporally interpolated model profiles to the instantaneous IASI observations at $\sim 10:30$ LT and then apply the averaging kernels.

Hindcast experiments of tropospheric composition

V. Huijnen et al.

Title Page

Abstract

Introduction

Conclusions

References

Tables

Figures



Back

Close

Full Screen / Esc

Printer-friendly Version

Interactive Discussion



Hindcast experiments of tropospheric composition

V. Huijnen et al.

Title Page

Abstract

Introduction

Conclusions

References

Tables

Figures

⏪

⏩

◀

▶

Back

Close

Full Screen / Esc

Printer-friendly Version

Interactive Discussion



In Fig. 8 we present maps of mean tropospheric O_3 partial columns. On average the model runs are all well in line with IASI over Western Europe, and show a slightly high bias over the Mediterranean region. All runs miss the high ozone columns south-east of Moscow and particularly over Western Kazakhstan, as observed by IASI. The reasons for this are not fully understood. Although no strong wildfires took place here, the heat wave extended into this region, with daytime maximum temperatures reaching 40°C in the first two weeks of August. This resulted in a reduction in ozone dry deposition flux due to low soil wetness levels. However, this is insufficient to explain the high levels of tropospheric ozone. The model might suffer from the same shortcomings as suggested in the evaluation of the 2003 heat wave over Western Europe (Ordóñez et al., 2010), i.e., the impact of high temperatures and increased solar radiation on the biogenic emissions (e.g., Lee et al., 2006; Solberg et al., 2008), which, together with moderately high NO_x concentrations, can increase O_3 production. Furthermore, a possible positive bias in the IASI retrieval could also contribute to the discrepancy between the model and observations. This bias could be caused by spectral interferences between ozone and aerosols and/or water vapor. Nevertheless, key spatial patterns are captured by the model, such as the north-south gradient in O_3 columns over Western Russia. Local differences between the runs are less than ~ 2 DU.

Figure 9 shows the time evolution of the corresponding area-mean tropospheric O_3 columns for hindcasts D + 0. It illustrates that all model runs are able to capture the increase in O_3 columns at the beginning of August, as well as the strong decrease between 10 and 21 August, the end of the heat wave. However, all model runs show a negative bias of ~ 2 – 4 DU with respect to IASI during the heat wave. This is largest for run CNT, and lowest for the runs that apply the GFAS emissions, indicating its positive impact on the ozone chemistry in the model.

The spatial variability in the instantaneous ozone columns is significantly larger for the IASI retrieval than in the model. While the daily average standard deviation of the IASI O_3 observations over Western Russia between 20 July and 15 August is 3.1 DU, it is only between 1.2 and 1.3 DU for the different hindcast runs. Part of this larger

Hindcast experiments of tropospheric composition

V. Huijnen et al.

Title Page

Abstract

Introduction

Conclusions

References

Tables

Figures

⏪

⏩

◀

▶

Back

Close

Full Screen / Esc

Printer-friendly Version

Interactive Discussion



standard deviation in IASI columns can be explained by retrieval errors, estimated to be ~ 2.5 DU for the given time period and region. Furthermore, a lack of variability in the modeled O_3 concentrations in the free troposphere contributes to this discrepancy. This strongly contributes to the RMSE of the model against the IASI observations, which ranges between 3.2 and 4.0 DU, see Table 6. Although the use of assimilation helps to reduce the model bias and RMSE, the largest improvement is a result of the use of the GFAS emissions, with a reduction of the mean bias (RMSE) of $\sim 38\%$ (13%) compared to the control run for D + 0. The relative difference between the error measures of the different hindcast runs is similar for all hindcast days, indicating the lasting effect of both initialization by assimilated fields as well as the use of GFAS emissions.

Despite the rather similar results for tropospheric O_3 columns between the various runs, there are significant differences in the planetary boundary layer (PBL). Figure 10 shows that surface O_3 concentrations are only slightly affected by the initialization from assimilation, while they are enhanced by $\sim 15\%$ when using the GFAS emissions during the time of the fires. Moreover the figure illustrates that hindcasts using the GFAS emissions lead to elevated O_3 levels throughout the troposphere while the assimilation has the largest impact at altitude levels between 600 and 300 hPa, and the smallest in the PBL, similar to what was found for CO. Irrespective of the missing effects of the aerosols, which would presumably lead to a reduction in surface ozone concentrations (Konovalov et al., 2011), this shows the relevance of the NRT emission estimates on the modeling of ozone concentrations in the PBL, compared to the impact of ozone assimilation.

3.2.4 Tropospheric nitrogen dioxide

We compare hindcasts of tropospheric NO_2 columns against the IUP Bremen SCIAMACHY NO_2 product. Air mass factors determined from radiative transfer calculations are used to convert slant to vertical columns (Richter et al., 2005). NO_2 tropospheric columns are only determined for clear sky pixels, a selection performed according

Hindcast experiments of tropospheric composition

V. Huijnen et al.

Title Page

Abstract

Introduction

Conclusions

References

Tables

Figures



Back

Close

Full Screen / Esc

Printer-friendly Version

Interactive Discussion

to FRESCO data (Koelemeijer et al., 2001, 2002) for cloud fractions smaller than 20%. Model data coinciding in time and space with SCIAMACHY measurements are used. The hindcasts are further compared to the DOMINO product v1.02 (Boersma et al., 2007), applying the same selection criteria as for SCIAMACHY, see also Huijnen et al. (2010b). Note that the same OMI NO₂ column data were also used in the assimilation system, to provide initial conditions for the runs Assim and Assim-GFAS.

In general, the various model runs compare well to the SCIAMACHY measurements over Western Russia, see Fig. 11. A hot-spot of high NO₂ columns is observed within the gridbox containing Moscow, which can mainly be attributed to anthropogenic emissions. Both the SCIAMACHY and OMI instruments detect a large region of intensified NO₂ spreading east of Moscow that is not simulated by any of the hindcast runs. Considering the size of this region this deficiency in the model simulations could point at uncertainties in the soil NO_x emissions. In the current inventory these contribute to ~20% of the total emissions in run GFAS (see Table 3).

In the surroundings of Moscow both SCIAMACHY and OMI show enhanced NO₂ columns that may be attributed to fire emissions. The hindcast run GFAS has on average higher columns compared to CNT within this region. However, run GFAS shows the spots of high NO₂ columns at different locations than observed from the satellite instruments. When switching on the initialization from assimilation, the NO₂ columns over Western Russia increase on average, thereby reducing the negative model bias. This is most visible in the region extending south and east of Moscow.

The scatter plots presented in Fig. 12 reveal in more detail the correlation between the different runs and the observations over Western Russia. The corresponding correlations and slopes as derived from a linear regression are given in Table 7. Surprisingly, the best correlations are obtained for the simulations with climatological emissions, indicating that the spatial distribution of the GFAS emissions indeed does not accurately reflect the actually observed variability in NO₂ columns.

Hindcast experiments of tropospheric composition

V. Huijnen et al.

[Title Page](#)[Abstract](#)[Introduction](#)[Conclusions](#)[References](#)[Tables](#)[Figures](#)[Back](#)[Close](#)[Full Screen / Esc](#)[Printer-friendly Version](#)[Interactive Discussion](#)

The largest outlier in the scatter plot against SCIAMACHY was obtained for the runs that use GFAS emissions and can be traced back to the model hindcast for 30 July. For this particular day emissions due to peat fires were extreme in a small region east of Moscow (see Fig. 2). Actual emissions for that day are highly uncertain as these were kept identical to the ones from the previous day (see Sect. 3.1).

The mean bias and RMSE for all hindcast days with respect to the SCIAMACHY and OMI NO₂ products are given in Tables 8 and 9. As expected, the mean bias decreases by 64 % (31 %) against SCIAMACHY (OMI) when using the GFAS emissions, but the RMSE significantly increases for the comparison with SCIAMACHY, while it hardly changed for OMI. Note that the observed variability due to retrieval errors will significantly contribute to the RMSE (Boersma et al., 2007). The remaining contribution to the RMSE can be attributed to a mismatch of the local emissions. The different time of the SCIAMACHY (10:00 LT) and OMI (13:30 LT) overpasses can partly explain the different results for the statistics. Compared to the afternoon, in the morning the NO₂ concentrations are generally higher (less photochemistry), with a potential larger spatial variability (less mixing), and, hence, the impact of the emissions on the variability in observed NO₂ columns is stronger than in the afternoon.

A reduction in the bias of 30 % (46 %) compared to SCIAMACHY (OMI) is achieved when including the assimilation of O₃, CO and NO₂ observations for initialization. The assimilation also leads to a slight decrease of the RMSE, which can be explained by the improved mean bias. Considering the short lifetime of NO₂, we cannot exclude that most of the impact of the assimilation on NO₂ is indirect, via assimilation of CO and O₃. This is also consistent with the persisting lower bias with increasing forecast length in the assimilation runs. The enhanced CO causes a reduced abundance of OH radicals in the troposphere (e.g., Duncan et al., 2003). This in turn inhibits the formation of nitric acid (HNO₃) by oxidation of NO₂. More tropospheric O₃ would furthermore lead to higher NO titration in favour of NO₂ production. Indeed the OH concentrations over the Moscow gridbox during the first 10 days in August decrease by ~ 5 % in the free troposphere in run Assim-GFAS versus run GFAS. Yet, the actual numbers vary

considerably depending on the hindcast day, altitude level and location. Further work is needed to quantify and validate the indirect effects of the assimilation on the chemical composition.

3.2.5 Formaldehyde

The retrieval of HCHO columns from the SCIAMACHY instrument follows a similar approach as described in the previous subsection for NO₂, and is further detailed in Wittrock (2006) and Wittrock et al. (2006). Offsets introduced by the solar reference measurements are compensated by normalizing the retrieved slant columns with a mean value of 3.5×10^{15} molec cm⁻² in the region between 180°–200° E. Airmass factors are used to convert the slant to vertical columns. These are taken from pre-calculated values that assumed a variable tropospheric aerosol loading. However, these scenarios do not necessarily represent the conditions of the fire event analyzed in this study. This means that a more precise correction of aerosol effect could lead to higher HCHO columns retrieved from SCIAMACHY observations (Wittrock, 2006). One other aspect to consider is that the low coverage of satellite pixels for SCIAMACHY data (combined with the short period of the analysis) implies a small number of measurements available per model grid box. This leads to a relatively large uncertainty in the averaged data due to the noise in the individual measurements, which in combination with the offset correction for some cases results in negative HCHO columns. Considering the low coverage also no cloud screening is performed for HCHO retrievals. The uncertainty in the mean of the observations is estimated of the order 10^{16} molec cm⁻² (Wittrock, 2006).

Figure 13 presents the modeled tropospheric HCHO columns and observations from SCIAMACHY. In these maps a spatial smoothing of the SCIAMACHY data has been applied to suppress the relatively large natural scatter in the HCHO observations. All model versions show somewhat higher HCHO background concentrations than observed from SCIAMACHY, which may partly be related to the offset correction in SCIAMACHY. On the other hand, the SCIAMACHY HCHO columns show a distinct region of

Hindcast experiments of tropospheric composition

V. Huijnen et al.

Title Page

Abstract

Introduction

Conclusions

References

Tables

Figures

⏪

⏩

◀

▶

Back

Close

Full Screen / Esc

Printer-friendly Version

Interactive Discussion



Hindcast experiments of tropospheric composition

V. Huijnen et al.

Title Page

Abstract

Introduction

Conclusions

References

Tables

Figures

⏪

⏩

◀

▶

Back

Close

Full Screen / Esc

Printer-friendly Version

Interactive Discussion



high HCHO columns east of Moscow. A similar hot-spot, although higher, is only identified in the model simulations where the updated GFAS emissions were considered. The indirect impact of the assimilation is marginal: HCHO columns are on average $\sim 0.3 \times 10^{15}$ molec cm⁻² lower compared to runs without initialization from assimilation.

This could be explained by the change in oxidative capacity in the model, related to the higher tropospheric NO_x, CO and O₃. Still, a large difference between the model runs that use the GFAS emissions and satellite data can be perceived, with the model having both higher background values as well as a different magnitude and shape of the region with elevated HCHO levels. This difference can be explained by uncertainties in both the model and the observations.

As the calculated bias and RMSE between model and observations are in this case strongly influenced by the scatter in the observations and the outliers, such an analysis does not lead to significant results. Here, we focus on the spatial correlation between the model results and the SCIAMACHY observations. For this calculation the original observational data has been used without smoothing. The HCHO scatter plot (Fig. 15) illustrates that, for the background concentrations, i.e., SCIAMACHY observations below 10¹⁶ molec cm⁻², the model shows approximately constant HCHO columns of 10¹⁶ molec cm⁻². Very similar results for the runs with/without assimilation are obtained. The presence of the region with high HCHO in the model runs with GFAS leads to a significant improvement in the slope of the regression and the correlation between the model and the SCIAMACHY observations, Table 10. This demonstrates the positive impact of the GFAS emissions on modeled HCHO columns. The large outlier in these runs with an average model column of 6.7×10^{16} is related to the peat fire emissions east of Moscow on 30 July, and corresponds to the outlier in the SCIAMACHY NO₂ scatter plot.

4 Integral assessment of GFAS emissions and assimilation on hindcasts

In this section we assess the integral impact of both the GFASv1.0 emissions and initialization by assimilated trace gases on the atmospheric composition at D + 0, focusing on the chemical interactions between the various trace gases. Also the implications of different start-conditions and emission estimates for the D + 1 to D + 3 hindcasts are analyzed.

4.1 Impact of fire emissions on chemical production and loss budgets

The impact on local production/loss budgets and the respective total masses (burdens) resulting from the application of the GFASv1.0 fire emissions as compared to the climatological emissions is given in Table 11. Note that the emission budgets include all contributing emission types in this region.

The modeled HCHO burden in run GFAS increases by 56 %, mainly due to the enhanced local HCHO emissions from GFASv1.0, but also because of enhanced oxidation of other hydrocarbons. Although the chemical production of CO, which is mainly driven by HCHO oxidation, increases by 22 % in run GFAS, the absolute contribution to the CO production remains small. About 4 % of the extra CO production in run GFAS can be attributed to GFASv1.0 emissions of HCHO and other higher hydrocarbons. Thus, 96 % of the increase in CO burden is attributed to the direct CO fire emissions. An indirect effect of the large GFASv1.0 emissions is an increase of 19 % in the local CO lifetime, calculated as the local burden over the chemical loss. This corresponds to a lifetime of 1.5 month in run GFAS, and is hence a significant contributor to enhanced CO concentrations in the troposphere. The increase in CO lifetime illustrates a reduction of the hydroxyl radical (OH) concentration, which also explains the reduced CH₄ oxidation budget. This is related to an increased scavenging of OH by the larger CO concentrations, as was discussed earlier by Duncan et al. (2003).

Additionally, the ozone chemical production and loss terms increase, related to larger NO_x and NMVOC emissions due to the fires. Overall a net increase in tropospheric O₃

Hindcast experiments of tropospheric composition

V. Huijnen et al.

Title Page

Abstract

Introduction

Conclusions

References

Tables

Figures



Back

Close

Full Screen / Esc

Printer-friendly Version

Interactive Discussion



**Hindcast
experiments of
tropospheric
composition**

V. Huijnen et al.

Title Page

Abstract

Introduction

Conclusions

References

Tables

Figures

⏪

⏩

◀

▶

Back

Close

Full Screen / Esc

Printer-friendly Version

Interactive Discussion

burden of 4 % is found. O_3 concentrations are mostly enhanced in the PBL, see also Sect. 3.2. The dry deposition velocities in the two runs are identical, as they depend on meteorology only. Therefore the increase in O_3 concentrations in the PBL explains the comparatively larger increase in O_3 dry deposition flux by 10%. As discussed earlier, the increase in the O_3 burden is insufficient compared to the IASI observations, suggesting an under-estimation of ozone precursor gas emissions.

The mean biases in NO_2 columns with respect to both SCIAMACHY and OMI, for the runs using the GFASv1.0 fire emissions, have improved significantly compared to the hindcast results with climatological emissions. This improvement suggests a general positive impact of higher NO_x emissions on the model results. Nevertheless, the evaluation still indicates an under-estimation of NO_x emissions, which could contribute to the low bias in O_3 .

Several authors suggested that an excess of aerosol concentrations will have an impact on chemical and photolysis rates, depending on aerosol microphysical and optical properties (e.g., Hodzic et al. 2007; Real et al., 2007; Verma et al., 2009). Konovalov et al. (2011) estimated that the neglect of shielding by an aerosol plume leads to a positive bias of ~ 20 – 50 % in O_3 at the surface layer over Moscow, during most days in the intense fire period. This was explained by an overestimation of the ozone production by NO_2 photolysis.

Overall we find that the increase in O_3 burden and the larger NO_x -recycling are insufficient to counterbalance the larger OH scavenging by CO. As we do not account for aerosol effects, the O_3 production is likely over-estimated, as well as primary OH production due to the ozone photolysis. Correspondingly, this implies an over-estimation of the local CH_4 and CO loss by oxidation. However, the magnitude of this effect is highly uncertain, depending on the actual aerosol optical parameters and the spatial and vertical distribution (Real et al., 2007). Also, while the effects can be very important on a local scale, as shown by Konovalov et al. (2011), their impact on the chemical budgets on a sub-continental scale is unclear, but likely small.

4.2 Impact of assimilation on chemical composition

The application of assimilation helps in most cases to reduce model biases. A small negative bias in CO with respect to MOPITT-V4 before and after the fire episode was found, whereas for days with the largest CO columns the hindcasts initialized with assimilated IASI CO show a high bias of $\sim 0.5 \times 10^{18}$ molec cm⁻². These biases are in line with an earlier evaluation for summer 2007 Greek fires (Turquety et al., 2009).

When switching on the assimilation of O₃ total and partial stratospheric columns the negative O₃ bias decreases by 19% compared to the control run, i.e., the impact is less than the application of GFASv1.0. This is understandable because the highest sensitivity of the instruments that provide data used in the assimilation is to the stratosphere. For NO₂ the assimilation is more effective, showing reductions in mean bias of 30% (46%) compared to SCIAMACHY (OMI). Also, the spatial correlation and the regression slope improves. Model HCHO columns are slightly lower with assimilation, as a consequence of a different oxidizing capacity of the atmosphere.

As in the current model runs CO, O₃ and NO₂ are assimilated simultaneously, it is difficult to assess from the D + 0 hindcasts the indirect impact of assimilation of one trace gas on the other, especially the interaction between NO₂ assimilation and the other trace gases. Studying this effect requires separate sensitivity studies.

4.3 impact of GFAS emissions and assimilation on D + 1 to D + 3 hindcasts

Generally the D + 1 to D + 3 forecast accuracy decreases with increasing lead time, but its rate differs depending on the model version and trace gas. The runs that use the climatological emissions show a more gradual decay in forecast accuracy than those with the daily varying GFASv1.0 emissions, mainly visible from the RMSE. This implies that in case GFASv1.0 is not used, the initial conditions, and hence the application of data assimilation, is more critical to the forecast accuracy. When looking at an error measure based on local data (AERONET AOD) compared to area-averaged measure this effect is even stronger. Also, the RMSE for NO₂ shows a decay in accuracy with

Hindcast experiments of tropospheric composition

V. Huijnen et al.

Title Page

Abstract

Introduction

Conclusions

References

Tables

Figures

⏪

⏩

◀

▶

Back

Close

Full Screen / Esc

Printer-friendly Version

Interactive Discussion



increasing forecast length, being ~ 50 % worse than a run without GFASv1.0 emissions at hindcast D + 3. This all shows that the RMSE is sensitive to the variability of the emissions, and this is lower for the model with climatological emissions.

On the other hand, when forecast error is defined as an area-average mean bias on a regional scale, hindcasts that include the GFASv1.0 emissions show generally better accuracy than those that are only initialized with concentration fields from the assimilation. For instance, the mean bias in CO total columns is reduced by 84 % at hindcast D + 3. This illustrates that the applied emission estimates become more relevant compared to the initialization, with increasing forecast time. For O₃, the RMSE and mean bias remain strongly linked to the values at hindcast D + 0, showing the lasting impact of the initial conditions. Also for NO₂ the negative mean bias at hindcast D + 3 stays smaller in the runs with assimilation compared to those without. Considering the rather short lifetime for NO₂ this suggests an indirect effect of the ozone and CO assimilation on NO₂, possibly due to a persistently reduced abundance of OH radicals in the troposphere. Best model performance is achieved with both assimilation and GFASv1.0 emissions switched on.

5 Summary and conclusions

Western Russia experienced a strong heat wave in the summer of 2010. Together with a drought, this resulted in severe wildfires which led to large-scale enhancements of trace gas and aerosol concentrations over several days. The fire emissions showed large variation in space and time, which aggravates the challenge to provide realistic forecasts of air pollution a few days in advance. In the framework of the MACC project a system has been developed for routine monitoring and forecasting of atmospheric composition on a global scale, whereby the meteorological data assimilation system at ECMWF has been extended with the assimilation of various reactive trace gases and aerosol optical depths. Fire emissions are available in near realtime from the GFASv1.0 system based on FRP data from the MODIS satellite instrument. We conducted a set

Hindcast experiments of tropospheric composition

V. Huijnen et al.

Title Page

Abstract

Introduction

Conclusions

References

Tables

Figures



Back

Close

Full Screen / Esc

Printer-friendly Version

Interactive Discussion



Hindcast experiments of tropospheric composition

V. Huijnen et al.

[Title Page](#)[Abstract](#)[Introduction](#)[Conclusions](#)[References](#)[Tables](#)[Figures](#)[⏪](#)[⏩](#)[◀](#)[▶](#)[Back](#)[Close](#)[Full Screen / Esc](#)[Printer-friendly Version](#)[Interactive Discussion](#)

of four model experiments with this system to quantify the effects of accurate and variable fire emissions and chemical data assimilation on the prediction of the chemical composition of the troposphere during July–August 2010 over Western Russia. In the current setup the aerosols are calculated within the IFS, and the reactive gases based on the coupled IFS-TM5 system.

The total emission of CO for the period 16 July to 15 August 2010 based on GFASv1.0 were 12.2 Tg of CO, which is about 11 times larger than the default emissions from a multi-annual climatology. An important factor for the accuracy of the fire emissions was the development of a detailed soil map for GFAS which contained the peatland areas east of Moscow, where some of the largest emissions originated from. Of the total CO emissions $\sim 20\%$ are attributed to peat fires. The GFASv1.0 CO emissions are $\sim 25\%$ larger than estimated by Konovalov et al. (2011). Taking into account the large uncertainties in wildfire emissions, we consider the agreement between the two approaches encouraging.

The assessment of the 0–24 h hindcasts revealed that the impact of the GFASv1.0 emissions is dominant on the composition in the boundary layer, whereas the assimilation system changes concentrations more evenly distributed over the troposphere, reflecting the coarse vertical resolution of the averaging kernels and the error covariance matrices of the satellite data. For instance, data assimilation increased surface CO concentrations by 33 % compared to the control run, while the additional impact of the application of GFASv1.0 was 55 %.

Even though similar tropospheric O₃ and CO columns were obtained with the assimilation system solely, the vertical attribution was highly dependent on the modeled first guess concentrations, and hence the fire emissions. Furthermore, besides the lack of vertical information, the assimilation of AOD encounters the difficulty of attributing the differences in observed and model AOD to the correct aerosol types. Therefore also the concentrations of the assimilated aerosol species were highly dependent on the modelled values. Actual fire emissions, which can change the ratio between, e.g., black carbon, sulphate and dust, are therefore crucial for the assimilation results. Hence the

GFASv1.0 emissions complement the assimilation system in regions, altitudes and for trace gases or aerosol components that are not affected by the assimilation.

With application of GFASv1 emissions, the 0–24 h hindcasts captured most of the individual events of high AOD, including the extreme event with values larger than 3.

Hindcasts of AOD, tropospheric CO, O₃ and NO₂ columns showed improvement in mean biases with respect to observations of 87, 63, 38 and 64 %, respectively, compared to the control run. By furthermore applying assimilation, the combined improvement for these compounds was 90, 87, 38 and 80 %. Better satellite observations, by increased accuracy and better spatial and temporal resolution, would be beneficial to further improve the accuracy of the 0–24 h hindcasts.

The application of GFASv1.0 emissions resulted in a constant bias in CO tropospheric columns of -0.3×10^{18} molec cm⁻² against the MOPITT-V4 observations, before, during and after the main event. This suggests accurate GFASv1.0 emission totals for CO. Remaining biases, which are mostly resolved with the initialization from assimilation, may be explained by other missing emission sources or model deficiencies (Huijnen et al., 2010a). The negative bias in tropospheric O₃ in all model runs with respect to IASI retrievals over the western part of Kazakhstan could possibly be explained by a combination of uncertainties in the retrieval and model errors, such as too low soil NO_x and/or biogenic VOC emissions due to heat wave conditions (Lee et al., 2006; Solberg et al., 2008). Despite the significant improvement in mean bias in NO₂ columns with respect to SCIAMACHY compared to the control run, the RMSE and correlation generally degraded with the application of GFASv1.0 emissions. This points at persisting local mismatches of the NO_x emission estimates, relevant due to the relatively short lifetime of NO_x. Correlations between SCIAMACHY HCHO and model hindcasts improved from $r^2 = 0.15$ to $r^2 = 0.42$ when using GFASv1.0 emissions. The rather poor spatial correlation is caused by the large scatter and low coverage in the observed HCHO column data, as well as HCHO model uncertainties, such as biogenic HCHO and other VOC emissions.

With the forecast accuracy defined as an area-average mean bias, the GFASv1.0

Hindcast experiments of tropospheric composition

V. Huijnen et al.

Title Page

Abstract

Introduction

Conclusions

References

Tables

Figures

⏪

⏩

◀

▶

Back

Close

Full Screen / Esc

Printer-friendly Version

Interactive Discussion



Hindcast experiments of tropospheric composition

V. Huijnen et al.

Title Page

Abstract

Introduction

Conclusions

References

Tables

Figures



Back

Close

Full Screen / Esc

Printer-friendly Version

Interactive Discussion



emissions are positively contributing to the hindcasts up to 96 h lead time, showing their relevance at the larger spatial scales. Furthermore, it is remarkable that the negative mean bias for NO₂ remains smaller for all hindcast days in the runs with assimilation compared to those without. These results suggest a positive indirect effect of the assimilation of long lived tracers (CO and O₃) on short lived ones, like NO₂.

On the other hand, the quality of local hindcasts depended strongly on the assumptions made for forecasted fire emissions. This was well visible from a relatively rapid decrease of the forecast accuracy, quantified by the RMSE with respect to ground-based data for AOD, and satellite based NO₂. The GFASv1.0 system simply propagates the observation-based emission estimates forward in time. This can lead to large overestimations of forecasted trace gas and aerosol concentrations when fire activity begins to subside after events of high emissions. In order to avoid false pollution alarms, a more sophisticated approach to forecast fire emissions based on the expected weather conditions and empirical analysis should be developed.

The combined analysis of fire radiative power observations, multiple trace gas and aerosol observations, as provided by the MACC system, result in a detailed quantitative description of the impact of major fires on atmospheric composition. Nevertheless, biases in the analysis remain significant for some trace gases, such as tropospheric ozone. Overall, this case study has demonstrated the capabilities of the MACC system to analyze air pollution during large-scale fire events and to forecast large-scale pollution plumes emanating from such fires. It highlights the necessity to maintain and improve the current capabilities for space-borne retrievals of trace gases, aerosols and fire radiative power.

Acknowledgements. We thank N. Chubarova and B. Holben and their staff for maintaining the Moscow AERONET site which provided data used in this investigation. Some of the satellite data were downloaded from the National Aeronautics and Space Administration (NASA) and the National Oceanic and Atmospheric Administration (NOAA). We acknowledge the free use of satellite retrieval data from www.temis.nl. The work has been carried out within the MACC project, which is funded by the European Commission under the Seventh Research Framework Programme.

References

- Akagi, S. K., Yokelson, R. J., Wiedinmyer, C., Alvarado, M. J., Reid, J. S., Karl, T., Crounse, J. D., and Wennberg, P. O.: Emission factors for open and domestic biomass burning for use in atmospheric models, *Atmos. Chem. Phys.*, 11, 4039–4072, doi:10.5194/acp-11-4039-2011, 2011.
- Andersson, E. and Järvinen, H.: Variational quality control, *Q. J. Roy. Meteor. Soc.*, 125, 697–722, 1999.
- Andreae, M. O. and Merlet, P.: Emission of trace gases and aerosols from biomass burning, *Global Biogeochem. Cy.*, 15(4), 955–966, 2001.
- Benedetti, A., Morcrette, J.-J., Boucher, O., Dethof, A., Engelen, R., Fisher, M., Flentje, H., Huneus, N., Jones, L., Kaiser, J., Kinne, S., Mangold, A., Razinger, M., Simmons, A., and Suttie, M.: Aerosol analysis and forecast in the European Centre for Medium-Range Weather Forecasts Integrated Forecast System: 2. Data assimilation, *J. Geophys. Res.*, 114, D13205, doi:10.1029/2008JD011115, 2009.
- Boersma, K. F., Eskes, H. J., Veefkind, J. P., Brinksma, E. J., van der A, R. J., Sneep, M., van den Oord, G. H. J., Levelt, P. F., Stammes, P., Gleason, J. F., and Bucsela, E. J.: Near-real time retrieval of tropospheric NO₂ from OMI, *Atmos. Chem. Phys.*, 7, 2103–2118, doi:10.5194/acp-7-2103-2007, 2007.
- Deeter, M. N., Edwards, D. P., Gille, J. C., Emmons, L. K., Francis, G., Ho, S.-P., Mao, D., Masters, D., Worden, Drummond, H. J. R., and Novelli, P. C.: The MOPITT version 4 CO product: Algorithm enhancements, validation, and long-term stability, *J. Geophys. Res.*, 115, D07306, doi:10.1029/2009JD013005, 2010.
- Dole, R., Hoerling, M., Perlwitz, J., Eischeid, J., Pegion, P., Zhang, T., Quan, X.-W., Xu, T., and Murray, D.: Was there a basis for anticipating the 2010 Russian heat wave?, *Geophys. Res. Lett.*, 38, L06702, doi:10.1029/2010GL046582, 2011.
- van Donkelaar, A., Martin, R. V., Levy, R. C., da Silva, A. M., Krzyzanowski, M., Chubarova, N. E., Semutnikova, E., and Cohen, A. J.: Satellite-based estimates of ground-level fine particulate matter during extreme events: a case study of the Moscow fires in 2010, *Atmos. Environ.*, 45(34), doi:10.1016/j.atmosenv.2011.07.068, 2011.
- Dufour, G., Eremenko, M., Griesfeller, A., Barret, B., LeFlochmoën, E., Clerbaux, C., Hadji-Lazaro, J., Coheur, P.-F., and Hurtmans, D.: Validation of three different scientific ozone products retrieved from IASI spectra using ozonesondes, *Atmos. Meas. Tech. Discuss.*, 4,

ACPD

11, 31851–31909, 2011

Hindcast experiments of tropospheric composition

V. Huijnen et al.

Title Page

Abstract

Introduction

Conclusions

References

Tables

Figures

⏪

⏩

◀

▶

Back

Close

Full Screen / Esc

Printer-friendly Version

Interactive Discussion



Hindcast experiments of tropospheric composition

V. Huijnen et al.

Title Page

Abstract

Introduction

Conclusions

References

Tables

Figures

⏪

⏩

◀

▶

Back

Close

Full Screen / Esc

Printer-friendly Version

Interactive Discussion

5425–5479, doi:10.5194/amtd-4-5425-2011, 2011.

Duncan, B. N., Bey, I., Chin, M., Mickley, L. J., Fairlie, T. D., Martin, R. V., and Matsueda, H.: Indonesian wildfires of 1997: Impact on tropospheric chemistry, *J. Geophys. Res.*, 108(D15), 4458, doi:10.1029/2002JD003195, 2003.

5 Elguindi, N., Clark, H., Ordóñez, C., Thouret, V., Flemming, J., Stein, O., Huijnen, V., Moinat, P., Inness, A., Peuch, V.-H., Stohl, A., Turquety, S., Athier, G., Cammas, J.-P., and Schultz, M.: Current status of the ability of the GEMS/MACC models to reproduce the tropospheric CO vertical distribution as measured by MOZAIC, *Geosci. Model Dev.*, 3, 501–518, doi:10.5194/gmd-3-501-2010, 2010.

10 FAO (Food and Agriculture Organization): WRB (World Reference Base) Map of World Soil Resources. Land and Water Development Division AGL, Food and Agriculture Organization of the United Nations, Rome, Italy, available online at: <http://www.fao.org/ag/agll/wrb/soilres.stm>, last access: 2 January 2004, 2003.

Flemming, J., Inness, A., Flentje, H., Huijnen, V., Moinat, P., Schultz, M. G., and Stein, O.: Coupling global chemistry transport models to ECMWF's integrated forecast system, *Geosci. Model Dev.*, 2, 253–265, doi:10.5194/gmd-2-253-2009, 2009.

Flemming, J., Inness, A., Jones, L., Eskes, H. J., Huijnen, V., Schultz, M. G., Stein, O., Carliolle, D., Kinnison, D., and Brasseur, G.: Forecasts and assimilation experiments of the Antarctic ozone hole 2008, *Atmos. Chem. Phys.*, 11, 1961–1977, doi:10.5194/acp-11-1961-2011, 2011.

20 George, M., Clerbaux, C., Hurtmans, D., Turquety, S., Coheur, P.-F., Pommier, M., Hadji-Lazaro, J., Edwards, D. P., Worden, H., Luo, M., Rinsland, C., and McMillan, W.: Carbon monoxide distributions from the IASI/METOP mission: evaluation with other space-borne remote sensors, *Atmos. Chem. Phys.*, 9, 8317–8330, doi:10.5194/acp-9-8317-2009, 2009.

25 Heil, A., Kaiser, J. W., van der Werf, G. R., Wooster, M. J., Schultz, M. G., and van der Gon, H. D.: Assessment of the real-time fire emissions (GFASv0) by MACC. Technical report 628, ECMWF, available at: <http://www.ecmwf.int/publications/library/do/references/show?id=89802> (Last access: November 2011), 2010.

30 Hodzic, A., Madronich, S., Bohn, B., Massie, S., Menut, L., and Wiedinmyer, C.: Wildfire particulate matter in Europe during summer 2003: meso-scale modeling of smoke emissions, transport and radiative effects, *Atmos. Chem. Phys.*, 7, 4043–4064, doi:10.5194/acp-7-4043-2007, 2007.

Hollingsworth, A., Engelen, R. J., Textor, C., Benedetti, A., Boucher, O., Chevallier, F., De-

Hindcast experiments of tropospheric composition

V. Huijnen et al.

Title Page

Abstract

Introduction

Conclusions

References

Tables

Figures

⏪

⏩

◀

▶

Back

Close

Full Screen / Esc

Printer-friendly Version

Interactive Discussion

thof, A., Elbern, H., Eskes, H., Flemming, J., Granier, C., Kaiser, J. W., Morcrette, J. J., Rayner, P., Peuch, V. H., Rouil, L., Schultz, M. G., Simmons, A. J., and The GEMS Consortium: The Global Earth-system Monitoring using Satellite and in-situ data (GEMS) Project: Towards a monitoring and forecasting system for atmospheric composition, *B. Am. Meteorol. Soc.*, 89(8), 1147–1164, doi:10.1175/2008BAMS2355.1, 2008.

Huijnen, V., Eskes, H. J., Poupkou, A., Elbern, H., Boersma, K. F., Foret, G., Sofiev, M., Valdebenito, A., Flemming, J., Stein, O., Gross, A., Robertson, L., D'Isidoro, M., Kioutsioukis, I., Friese, E., Amstrup, B., Bergstrom, R., Strunk, A., Vira, J., Zyryanov, D., Maurizi, A., Melas, D., Peuch, V.-H., and Zerefos, C.: Comparison of OMI NO₂ tropospheric columns with an ensemble of global and European regional air quality models, *Atmos. Chem. Phys.*, 10, 3273–3296, doi:10.5194/acp-10-3273-2010, 2010b.

Huijnen, V., Williams, J., van Weele, M., van Noije, T., Krol, M., Dentener, F., Segers, A., Houweling, S., Peters, W., de Laat, J., Boersma, F., Bergamaschi, P., van Velthoven, P., Le Sager, P., Eskes, H., Alkemade, F., Scheele, R., Nédélec, P., and Pätz, H.-W.: The global chemistry transport model TM5: description and evaluation of the tropospheric chemistry version 3.0, *Geosci. Model Dev.*, 3, 445–473, doi:10.5194/gmd-3-445-2010, 2010a.

Ichoku, C. and Kaufman, Y. J.: A method to derive smoke emission rates from MODIS fire radiative energy measurements, *IEEE Geosci. Remote S.*, 43, 2636–2649, 2005.

Kaiser, J. W., Suttie, M., Flemming, J., Morcrette, J.-J., Boucher, O., and Schultz, M. G.: Global real-time fire emission estimates based on space-borne fire radiative power observations, *AIP Conf. Proc.*, 1100, 645–648, doi:10.1063/1.3117069, 2009.

Kaiser, J. W., Heil, A., Andreae, M. O., Benedetti, A., Chubarova, N., Jones, L., Morcrette, J.-J., Razinger, M., Schultz, M. G., Suttie, M., and van der Werf, G. R.: Biomass burning emissions estimated with a global fire assimilation system based on observed fire radiative power, *Biogeosciences Discuss.*, 8, 7339–7398, doi:10.5194/bgd-8-7339-2011, 2011.

Inness, A., Flemming, J., Suttie, M., and Jones, L.: GEMS data assimilation system for chemically reactive gases. Technical report 587, ECMWF, available at: <http://www.ecmwf.int/publications/library/do/references/show?id=89131> (Last access: November 2011), 2009.

Konovalov, I. B., Beekmann, M., Kuznetsova, I. N., Yurova, A., and Zvyagintsev, A. M.: Atmospheric impacts of the 2010 Russian wildfires: integrating modelling and measurements of an extreme air pollution episode in the Moscow region, *Atmos. Chem. Phys.*, 11, 10031–10056, doi:10.5194/acp-11-10031-2011, 2011.

Lee, J. D., Lewis, A. C., Monks, P. S., Jacob, M. Hamilton, J. F., Hopkins, J. R., Watson, N. M.,

Hindcast experiments of tropospheric composition

V. Huijnen et al.

Title Page

Abstract

Introduction

Conclusions

References

Tables

Figures

⏪

⏩

◀

▶

Back

Close

Full Screen / Esc

Printer-friendly Version

Interactive Discussion

Saxtona, J. E., Ennis, C., Carpenter, L. J. Carslaw, N., Fleming, Z., Bandy, B. J., Oram, D. E., Penkett, S. A., Slemr, J., Norton, E., Rickard, A. R., Whalley, L. K., Heard, D. E., Bloss, W. J., Gravestock, T., Smith, S. C., Stanton, J., Pilling, M. J., Jenkin, M. E.: Ozone photochemistry and elevated isoprene during the UK heatwave of August 2003, *Atmos. Environ.*, 40, 7598–7613, 2006.

Matsueda, M.: Predictability of Euro-Russian blocking in summer of 2010, *Geophys. Res. Lett.*, 38, L06801, doi:10.1029/2010GL046557, (2011).

Mebust, A. K., Russell, A. R., Hudman, R. C., Valin, L. C., and Cohen, R. C.: Characterization of wildfire NO_x emissions using MODIS fire radiative power and OMI tropospheric NO₂ columns, *Atmos. Chem. Phys.*, 11, 5839–5851, doi:10.5194/acp-11-5839-2011, 2011.

Menut, L. and Bessagnet, B.: Atmospheric composition forecasting in Europe, *Ann. Geophys.*, 28, 61–74, doi:10.5194/angeo-28-61-2010, 2010.

Morcrette, J. J., Boucher, O., Jones, L., Salmond, D., Bechtold, P., Beljaars, A., Benedetti, A., Bonet, A., Kaiser, J. W., Razinger, M., Schulz, M., Serrar, S., Simmons, A. J., Sofiev, M., Suttie, M., Tompkins, A. M., and Untch, A.: Aerosol analysis and forecast in the European Centre for Medium-Range Weather Forecasts Integrated Forecast System: Forward modeling, *J. Geophys. Res.-Atmos.*, 114, D06206, doi:10.1029/2008JD011235, 2009.

Ordóñez, C., Elguindi, N., Stein, O., Huijnen, V., Flemming, J., Inness, A., Flentje, H., Karagkou, E., Moinat, P., Peuch, V.-H., Segers, A., Thouret, V., Athier, G., van Weele, M., Zerefos, C. S., Cammas, J.-P., and Schultz, M. G.: Global model simulations of air pollution during the 2003 European heat wave, *Atmos. Chem. Phys.*, 10, 789–815, doi:10.5194/acp-10-789-2010, 2010.

Real, E., Law, K. S., Weinzierl, B., Fiebig, M., Petzold, A. Wild, O. Methven, J., Arnold, S., Stohl, A., Huntrieser, H., Roiger, A., Schlager, H., Stewart, D., Avery, M., Sachse, G., Browell, E., Ferrare, R., and Blake, D.: Processes influencing ozone levels in Alaskan forest fire plumes during longrange transport over the North Atlantic, *J. Geophys. Res.*, 112, D10S41, doi:10.1029/2006JD007576, 2007.

Redler, R., Valcke, S., and Ritzdorf, H.: OASIS4 – a coupling software for next generation earth system modelling, *Geosci. Model Dev.*, 3, 87–104, doi:10.5194/gmd-3-87-2010, 2010.

Richter, A., Burrows, J. P., Nüß, H., Granier, C., and Niemeier, U.: Increase in tropospheric nitrogen dioxide levels over China observed from space, *Nature*, 437, 129–132, 2005.

Solberg, S., Hov, Ø., Søvde, A., Isaksen, I. S. A., Coddeville, P., De Backer, H., Forster, C., Orsolini, Y., and Uhse, K.: European surface ozone in the extreme summer 2003, *J. Geophys.*

Hindcast experiments of tropospheric composition

V. Huijnen et al.

Title Page

Abstract

Introduction

Conclusions

References

Tables

Figures

◀

▶

◀

▶

Back

Close

Full Screen / Esc

Printer-friendly Version

Interactive Discussion

Res., 113, D07307, doi:10.1029/2007JD009098, 2008

Stavrakou, T., Müller, J.-F., De Smedt, I., Van Roozendaal, M., van der Werf, G. R., Giglio, L., and Guenther, A.: Evaluating the performance of pyrogenic and biogenic emission inventories against one decade of space-based formaldehyde columns, *Atmos. Chem. Phys.*, 9, 1037–1060, doi:10.5194/acp-9-1037-2009, 2009.

Stiller, G. P.: with contributions from v. Clarmann, T., Dudhia, A., Echle, G., Funke, B., Glatthor, N., Hase, F., Höpfner, M., Kellmann, S., Kemnitzer, H., Kuntz, M., Linden, A., Linder, M., Stiller, G. P., and Zorn, S.: The Karlsruhe Optimized and Precise Radiative Transfer Algorithm (KOPRA), vol. FZKA 6487 of Wissenschaftliche Berichte, Forschungszentrum Karlsruhe, Germany, 2000.

Stolbovoi, V. and Savin, I.: Maps of soil characteristics, in: Land Resources of Russia. Laxenburg, Austria, edited by: Stolbovoi, V. and McCallum, I., International Institute for Applied Systems Analysis and the Russian Academy of Science, CD-ROM, Distributed by the National Snow and Ice Data Center/World Data Center for Glaciology, Boulder, 2002.

Turquety, S., Hurtmans, D., Hadji-Lazaro, J., Coheur, P.-F., Clerbaux, C., Josset, D., and Tsamalis, C.: Tracking the emission and transport of pollution from wildfires using the IASI CO retrievals: analysis of the summer 2007 Greek fires, *Atmos. Chem. Phys.*, 9, 4897–4913, doi:10.5194/acp-9-4897-2009, 2009.

Val Martin, M., Logan, J. A., Kahn, R. A., Leung, F.-Y., Nelson, D. L., and Diner, D. J.: Smoke injection heights from fires in North America: analysis of 5 years of satellite observations, *Atmos. Chem. Phys.*, 10, 1491–1510, doi:10.5194/acp-10-1491-2010, 2010.

van der Werf, G. R., Randerson, J. T., Giglio, L., Collatz, G. J., Kasibhatla, P. S., and Arellano Jr., A. F.: Interannual variability in global biomass burning emissions from 1997 to 2004, *Atmos. Chem. Phys.*, 6, 3423–3441, doi:10.5194/acp-6-3423-2006, 2006.

van der Werf, G. R., Randerson, J. T., Giglio, L., Collatz, G. J., Mu, M., Kasibhatla, P. S., Morton, D. C., DeFries, R. S., Jin, Y., and van Leeuwen, T. T.: Global fire emissions and the contribution of deforestation, savanna, forest, agricultural, and peat fires (1997–2009), *Atmos. Chem. Phys.*, 10, 11707–11735, doi:10.5194/acp-10-11707-2010, 2010.

Vautard, R., Honoreé, C., Beekmann, M., and Rouil, L.: Simulation of ozone during the August 2003 heat wave and emission control scenarios, *Atmos. Environ.*, 39, 2957–2967, 2005.

Verma, S., Worden, J., Pierce, B., Jones, D. B. A., Al-Saadi, J., Boersma, F., Bowman, K., Eldering, A., Fisher, B., Jourdain, L., Kulawik, S., and Worden, H.: Ozone production in boreal fire smoke plumes using observations from the Tropospheric Emission Spectrometer and the

Hindcast experiments of tropospheric composition

V. Huijnen et al.

Title Page

Abstract

Introduction

Conclusions

References

Tables

Figures

⏪

⏩

◀

▶

Back

Close

Full Screen / Esc

Printer-friendly Version

Interactive Discussion

Ozone Monitoring Instrument, *J. Geophys. Res.*, 114, D02303, doi:10.1029/2008JD010108, 2009.

Wiedinmyer, C., Akagi, S. K., Yokelson, R. J., Emmons, L. K., Al-Saadi, J. A., Orlando, J. J., and Soja, A. J.: The Fire INventory from NCAR (FINN): a high resolution global model to estimate the emissions from open burning, *Geosci. Model Dev.*, 4, 625–641, doi:10.5194/gmd-4-625-2011, 2011.

Witte, J. C., Douglass, A. R., da Silva, A., Torres, O., Levy, R., and Duncan, B. N.: NASA A-Train and Terra observations of the 2010 Russian wildfires, *Atmos. Chem. Phys.*, 11, 9287–9301, doi:10.5194/acp-11-9287-2011, 2011.

Wittrock, F.: The retrieval of oxygenated volatile organic compounds by remote sensing techniques, PhD thesis, University of Bremen, May 2006.

Wittrock, F., Richter, A., Oetjen, H., Burrows, J. P., Kanakidou, M., Myriokefalitakis, S., Volkamer, R., Beirle, S., Platt, U., and Wagner, T.: Simultaneous global observations of glyoxal and formaldehyde from space, *Geophys. Res. Lett.*, 33, L16804, doi:10.1029/2006GL026310, 2006.

Wooster, M. J., Roberts, G., Perry, G. L. W., and Kaufman, Y. J.: Retrieval of biomass combustion rates and totals from fire radiative power observations: FRP derivation and calibration relationships between biomass consumption and fire radiative energy release, *J. Geophys. Res.*, 110, D24311, doi:10.1029/2005JD006318, 2005.

Yurganov, L. N., Rakitin, V., Dzhola, A., August, T., Fokeeva, E., George, M., Gorchakov, G., Grechko, E., Hannon, S., Karpov, A., Ott, L., Semutnikova, E., Shumsky, R., and Strow, L.: Satellite- and ground-based CO total column observations over 2010 Russian fires: accuracy of top-down estimates based on thermal IR satellite data, *Atmos. Chem. Phys.*, 11, 7925–7942, doi:10.5194/acp-11-7925-2011, 2011.

Hindcast experiments of tropospheric composition

V. Huijnen et al.

Title Page

Abstract

Introduction

Conclusions

References

Tables

Figures

◀

▶

◀

▶

Back

Close

Full Screen / Esc

Printer-friendly Version

Interactive Discussion

Table 1. Summary of satellite data used in the assimilation. Blacklist criteria: variational quality control (QC), Solar Elevation (SOE) and latitude (LAT).

Species	Instrument	Satellite	Data product	Averaging kernels used	Blacklist criteria
CO	IASI	METOP-A	Total column	yes	QC > 0
O ₃	SCIAMACHY	ENVISAT	Total column	no	QC > 0 SOE < 6°
O ₃	OMI	AURA	Total column	no	QC > 0 SOE < 10°
O ₃	SBUV/2	NOAA-17, NOAA-18	Partial column	no	QC > 0 SOE < 6°
O ₃	MLS	AURA	Profiles	no	QC > 0
NO ₂	OMI	AURA	Tropospheric column	yes	QC > 0 LAT < 60° S LAT > 60° N
AOD	MODIS	AQUA, TERRA	Total column	no	LAT < 70° S LAT > 70° N

Hindcast experiments of tropospheric composition

V. Huijnen et al.

Title Page

Abstract

Introduction

Conclusions

References

Tables

Figures

⏪

⏩

◀

▶

Back

Close

Full Screen / Esc

Printer-friendly Version

Interactive Discussion

Table 2. Definition of model configurations.

Configuration	Initial conditions from assimilation	Biomass burning emissions
CNT	No	GFEDv2-clim
GFAS	No	GFASv1.0
Assim	Yes	GFEDv2-clim
Assim-GFAS	Yes	GFASv1.0

Hindcast experiments of tropospheric composition

V. Huijnen et al.

Title Page

Abstract

Introduction

Conclusions

References

Tables

Figures

⏪

⏩

◀

▶

Back

Close

Full Screen / Esc

Printer-friendly Version

Interactive Discussion



Table 3. Emission totals over Western Russia for daily GFASv1.0, GFEDv3 monthly emissions, the GFEDv2 climatological emissions, as well as anthropogenic and biogenic emissions as used in the hindcast runs. Anthropogenic emissions are from RETRO (Schultz et al., 2007) and biogenic emissions from GEIA (Guenter et al., 2005) for CO and from ORCHIDEE (Latière et al., 2006) for NO_x and HCHO.

	Period	1–15/7	16–31/7	1–15/8	16–31/8
BC (Gg C)	GFASv1.0	2.4	5.4	7.9	1.6
	GFEDv3.1	3.8	4.0	6.4	6.8
	GFEDv2 clim	3.2	3.5	4.1	4.4
	Anthropogenic	2.4	2.6	2.7	2.9
CO (Tg CO)	GFASv1.0	0.45	5.2	7.0	0.67
	GFEDv3.1	0.65	0.69	1.1	1.2
	GFEDv2 clim	0.50	0.53	0.60	0.64
	Anthropogenic	0.29	0.31	0.33	0.36
	Biogenic	0.43	0.46	0.38	0.40
NO _x (Gg NO)	GFASv1.0	8	29	42	6
	GFEDv3.1	19	20	35	38
	GFEDv2 clim	17	18	21	22
	Anthropogenic	47	50	52	55
	Soil	22	24	22	23
HCHO (Gg HCHO)	GFASv1.0	5.3	43.7	60.6	7.3
	GFEDv3.1	9.9	10.6	18.8	20.1
	GFEDv2 clim	–	–	–	–
	Anthropogenic	11	12	11	12

Hindcast experiments of tropospheric composition

V. Huijnen et al.

Table 4. Mean bias and RMSE of modeled AOD compared to the measurements from AERONET station at Moscow, between 20 July and 15 August, as function of the hindcast day.

Model	Mean bias				RMSE			
	D + 0	D + 1	D + 2	D + 3	D + 0	D + 1	D + 2	D + 3
CNT	−0.83	−0.79	−0.78	−0.73	0.85	0.81	0.79	0.75
GFAS	−0.10	−0.28	−0.14	0.12	0.56	0.45	0.64	0.74
Assim	−0.41	−0.51	−0.51	−0.48	0.45	0.54	0.55	0.52
Assim-GFAS	0.08	−0.05	0.02	0.27	0.43	0.41	0.54	0.77

Title Page

Abstract

Introduction

Conclusions

References

Tables

Figures

⏪

⏩

◀

▶

Back

Close

Full Screen / Esc

Printer-friendly Version

Interactive Discussion

Hindcast experiments of tropospheric composition

V. Huijnen et al.

Table 5. Mean bias and RMSE of modeled total CO columns (units 10^{18} molec cm^{-2}) compared to MOPITT V4 observations over Western Russia between 20 July and 15 August, as function of the hindcast day.

Model	Bias				RMSE			
	D + 0	D + 1	D + 2	D + 3	D + 0	D + 1	D + 2	D + 3
CNT	-0.79	-0.78	-0.78	-0.77	0.91	0.91	0.90	0.90
GFAS	-0.29	-0.27	-0.26	-0.22	0.52	0.53	0.57	0.64
Assim	0.13	-0.04	-0.20	-0.31	0.38	0.39	0.43	0.51
Assim-GFAS	0.10	0.04	-0.02	-0.05	0.40	0.46	0.54	0.62

Title Page

Abstract

Introduction

Conclusions

References

Tables

Figures

⏪

⏩

◀

▶

Back

Close

Full Screen / Esc

Printer-friendly Version

Interactive Discussion

Hindcast experiments of tropospheric composition

V. Huijnen et al.

Table 6. Mean bias and RMSE of modeled O₃ partial columns (0–6 km) in DU, compared to IASI O₃ observations over Western Russia between 20 July and 15 August, as function of the hindcast day.

Model	Bias				RMSE			
	D + 0	D + 1	D + 2	D + 3	D + 0	D + 1	D + 2	D + 3
CNT	–2.6	–2.6	–2.7	–2.7	3.8	3.7	3.9	4.0
GFAS	–1.6	–1.7	–1.8	–1.8	3.3	3.3	3.4	3.5
Assim	–2.1	–2.2	–2.3	–2.4	3.5	3.5	3.6	3.7
Assim-GFAS	–1.6	–1.7	–1.8	–1.9	3.2	3.3	3.3	3.5

Title Page

Abstract

Introduction

Conclusions

References

Tables

Figures

⏪

⏩

◀

▶

Back

Close

Full Screen / Esc

Printer-friendly Version

Interactive Discussion

Hindcast experiments of tropospheric composition

V. Huijnen et al.

Table 7. Slope and correlation (r^2) of modeled tropospheric NO_2 columns for hindcast D + 0 with respect to SCIAMACHY and OMI observations over Western Russia between 20 July and 15 August.

Model	Slope		r^2	
	SCIA	OMI	SCIA	OMI
CNT	0.53	0.41	0.63	0.89
GFAS	0.69	0.50	0.34	0.81
Assim	0.58	0.53	0.67	0.93
Assim-GFAS	0.74	0.62	0.39	0.89

Title Page

Abstract

Introduction

Conclusions

References

Tables

Figures

⏪

⏩

◀

▶

Back

Close

Full Screen / Esc

Printer-friendly Version

Interactive Discussion

Hindcast experiments of tropospheric composition

V. Huijnen et al.

Table 8. Mean bias and RMSE of modeled tropospheric NO₂ columns (units 10¹⁵ molec cm⁻²), compared to SCIAMACHY observations over Western Russia between 20 July and 15 August, as function of the hindcast day.

Model	Bias				RMSE			
	D + 0	D + 1	D + 2	D + 3	D + 0	D + 1	D + 2	D + 3
CNT	-0.36	-0.36	-0.36	-0.35	0.63	0.64	0.64	0.64
GFAS	-0.13	-0.15	-0.16	-0.14	0.90	0.87	0.90	0.97
Assim	-0.25	-0.29	-0.31	-0.32	0.61	0.62	0.63	0.64
Assim-GFAS	-0.07	-0.10	-0.12	-0.11	0.86	0.87	0.91	0.99

Title Page

Abstract

Introduction

Conclusions

References

Tables

Figures

⏪

⏩

◀

▶

Back

Close

Full Screen / Esc

Printer-friendly Version

Interactive Discussion

Hindcast experiments of tropospheric composition

V. Huijnen et al.

Table 9. Mean bias and RMSE of modeled tropospheric NO₂ columns (units 10¹⁵ molec cm⁻²), compared to OMI observations over Western Russia between 20 July and 15 August, as function of the hindcast day.

Run	Bias				RMSE			
	D + 0	D + 1	D + 2	D + 3	D + 0	D + 1	D + 2	D + 3
CNT	-0.35	-0.35	-0.35	-0.34	0.21	0.21	0.21	0.21
GFAS	-0.24	-0.25	-0.24	-0.23	0.20	0.20	0.20	0.20
Assim	-0.19	-0.24	-0.27	-0.28	0.18	0.19	0.19	0.20
Assim-GFAS	-0.16	-0.20	-0.22	-0.21	0.18	0.19	0.19	0.20

Title Page

Abstract

Introduction

Conclusions

References

Tables

Figures

⏪

⏩

◀

▶

Back

Close

Full Screen / Esc

Printer-friendly Version

Interactive Discussion

**Hindcast
experiments of
tropospheric
composition**

V. Huijnen et al.

Title Page

Abstract

Introduction

Conclusions

References

Tables

Figures

I◀

▶I

◀

▶

Back

Close

Full Screen / Esc

Printer-friendly Version

Interactive Discussion

Table 10. Slope and correlation (r^2) of modeled HCHO columns for hindcast D + 0 with respect to SCIAMACHY observations over Western Russia between 20 July and 15 August.

Model	Slope	r^2
CNT	0.15	0.15
GFAS	0.94	0.42
Assim	0.14	0.13
Assim-GFAS	0.91	0.39

Table 11. CO, HCHO and O₃ tropospheric chemical budgets in Tg, for runs CNT and GFAS, and the relative change expressed as (GFAS-CNT)/(CNT), calculated for the period 15 July–15 August over Western Russia. The imbalance in the HCHO, CO and O₃ budgets corresponds to the net mass change.

Model	CNT	GFAS	Difference (%)
HCHO emission	0.14	0.24	71
HCHO chem. prod	1.85	2.25	16
HCHO chem. loss	-1.80	-2.23	22
HCHO dry/wet deposition	-0.13	-0.17	31
HCHO net transport	-0.06	-0.09	-
HCHO burden	0.016	0.025	56
CO emission	2.4	13.5	463
CO chem. production	1.8	2.2	22
CO chem. loss	-2.2	-2.9	32
CO net transport	-2.2	-14.0	-
CO burden	2.8	4.4	57
CH ₄ loss	0.47	0.43	-9
NO _x emission (Tg N)	0.087	0.120	38
O ₃ chem production	6.8	8.4	24
O ₃ chem loss	-4.9	-5.5	12
O ₃ dry deposition	-2.15	-2.36	10
O ₃ net transport	-0.1	-1.0	-
O ₃ burden	3.64	3.80	4

Hindcast experiments of tropospheric composition

V. Huijnen et al.

Title Page

Abstract

Introduction

Conclusions

References

Tables

Figures

⏪

⏩

◀

▶

Back

Close

Full Screen / Esc

Printer-friendly Version

Interactive Discussion

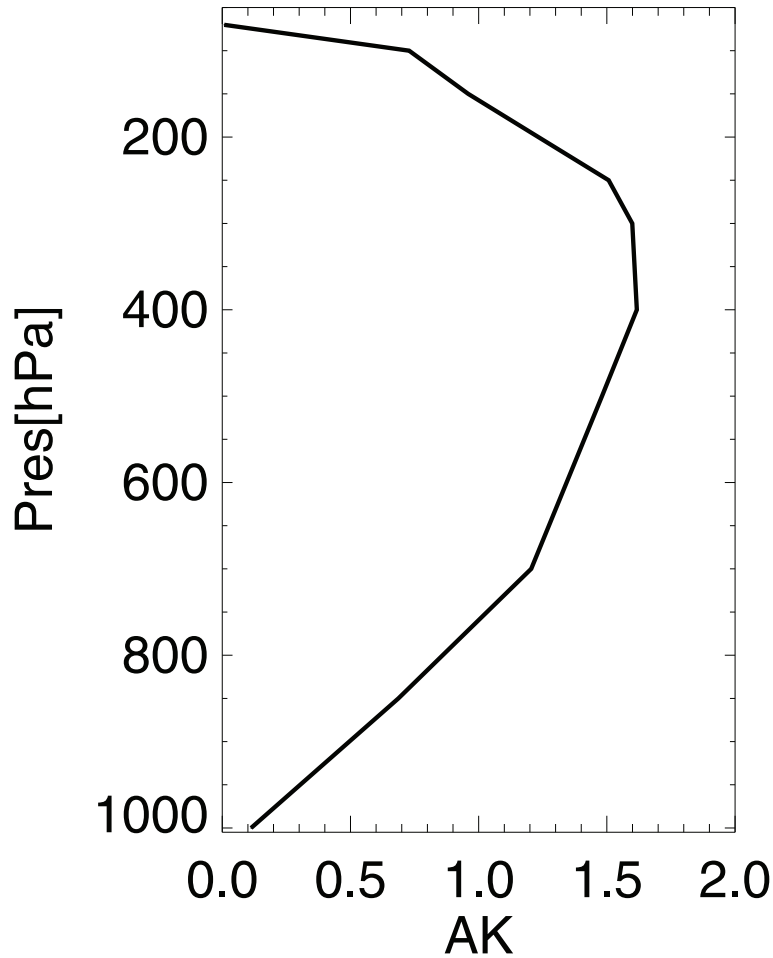


Fig. 1. Mean averaging kernel for IASI CO total columns over Western Russia for 20 July–15 August 2010.

Hindcast experiments of tropospheric composition

V. Huijnen et al.

[Title Page](#)

[Abstract](#) | [Introduction](#)

[Conclusions](#) | [References](#)

[Tables](#) | [Figures](#)

[⏪](#) | [⏩](#)

[◀](#) | [▶](#)

[Back](#) | [Close](#)

[Full Screen / Esc](#)

[Printer-friendly Version](#)

[Interactive Discussion](#)



Hindcast
experiments of
tropospheric
composition

V. Huijnen et al.

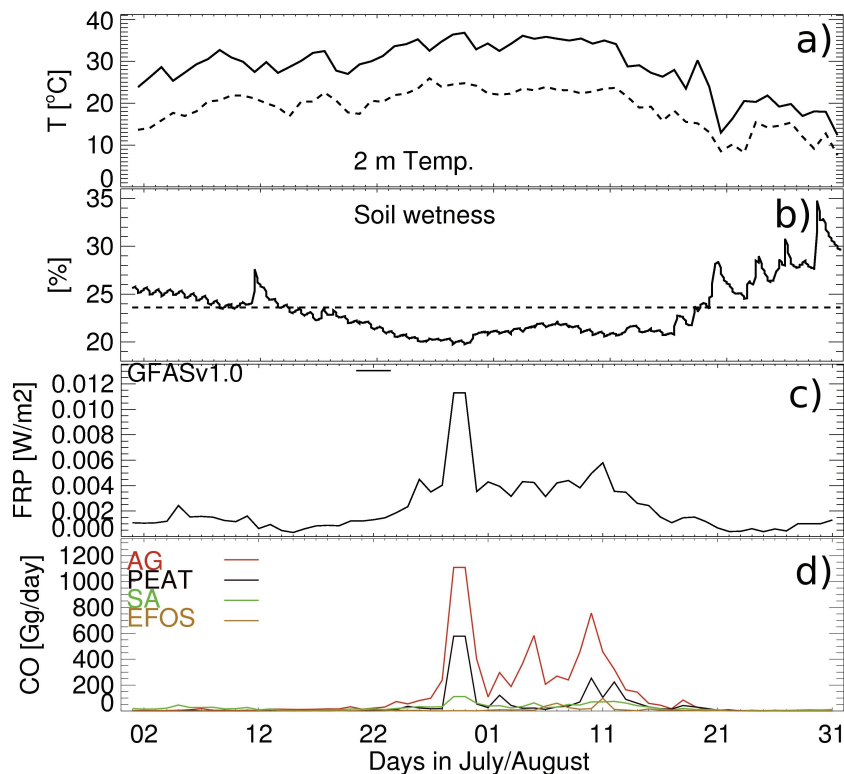


Fig. 2. Time series of **(a)** 2 m daily maximum (solid) and minimum (dashed) temperature, and **(b)** soil wetness at a location east of Moscow (42° E, 55° N) from ERA-Interim meteorology. The dashed line indicates the critical soil wetness level below which water stress takes place. Also shown are the **(c)** GFASv1.0 FRP product averaged over Western Russia, and **(d)** GFASv1.0 CO emissions over Western Russia aggregated per fuel type. Only emissions from the four dominant fuel types are shown: AG: Agriculture, PEAT: Peat soils (histosols), SA: Savanna, EFOS: Extratropical forest (with partial burning of organic soil matter).

[Title Page](#)[Abstract](#)[Introduction](#)[Conclusions](#)[References](#)[Tables](#)[Figures](#)[◀](#)[▶](#)[◀](#)[▶](#)[Back](#)[Close](#)[Full Screen / Esc](#)[Printer-friendly Version](#)[Interactive Discussion](#)

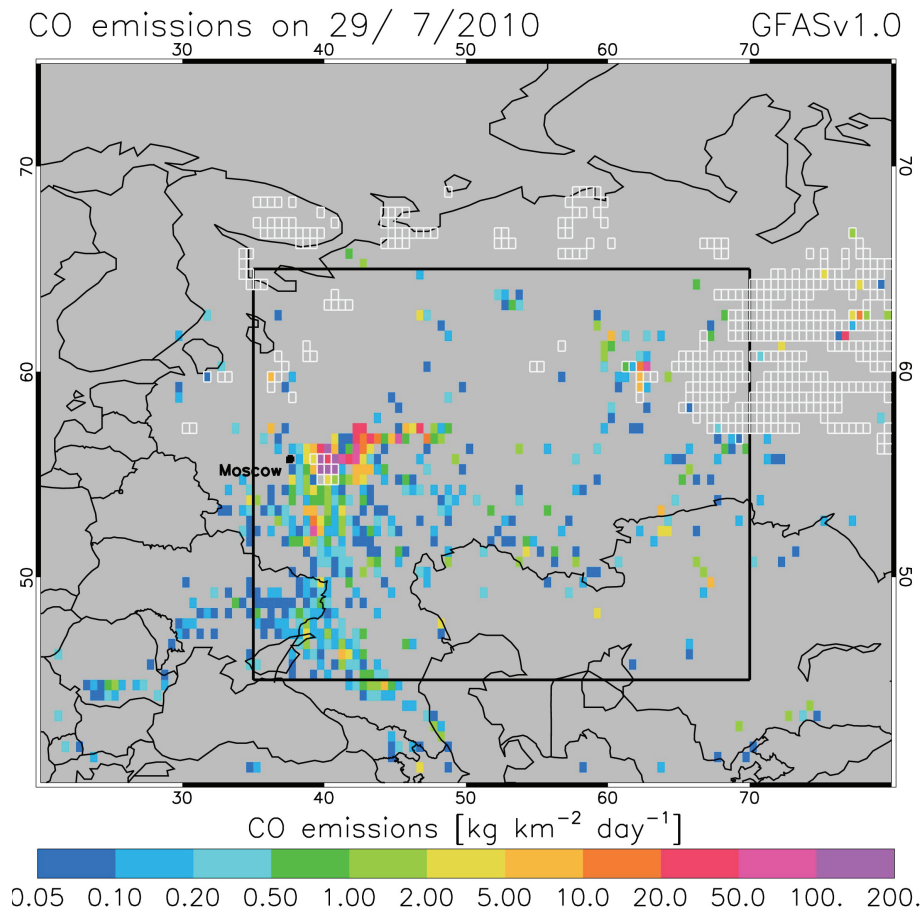


Fig. 3. Snapshot of CO emissions from GFASv1.0 on 29 July 2010. The white boxes indicate areas with peat soil as the dominant land cover type. Also indicated is the Western Russia region (35° E–70° E x 45° N–65° N).

Hindcast
experiments of
tropospheric
composition

V. Huijnen et al.

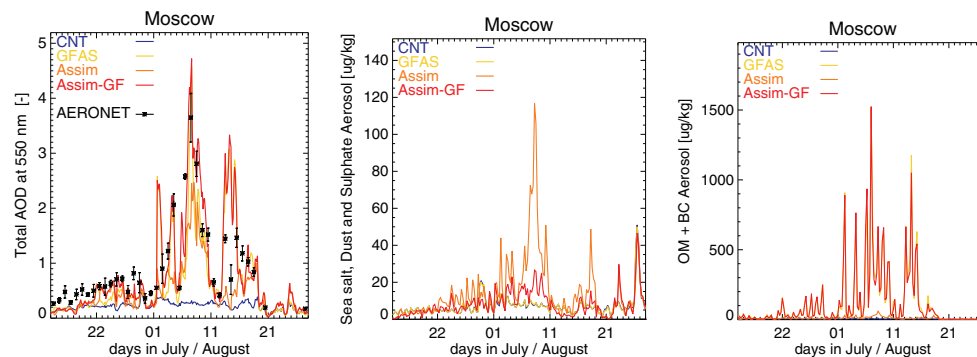


Fig. 4. (Left) modeled total aerosol optical depth at D + 0, compared to daily average AERONET observations at the Moscow station (black). The error bars reflect the daily variance in the available observations. (Middle) total of seasalt, dust and sulphate aerosol. (Right) total of organic matter and black carbon aerosol.

Title Page

Abstract

Introduction

Conclusions

References

Tables

Figures

◀

▶

◀

▶

Back

Close

Full Screen / Esc

Printer-friendly Version

Interactive Discussion

Hindcast experiments of tropospheric composition

V. Huijnen et al.

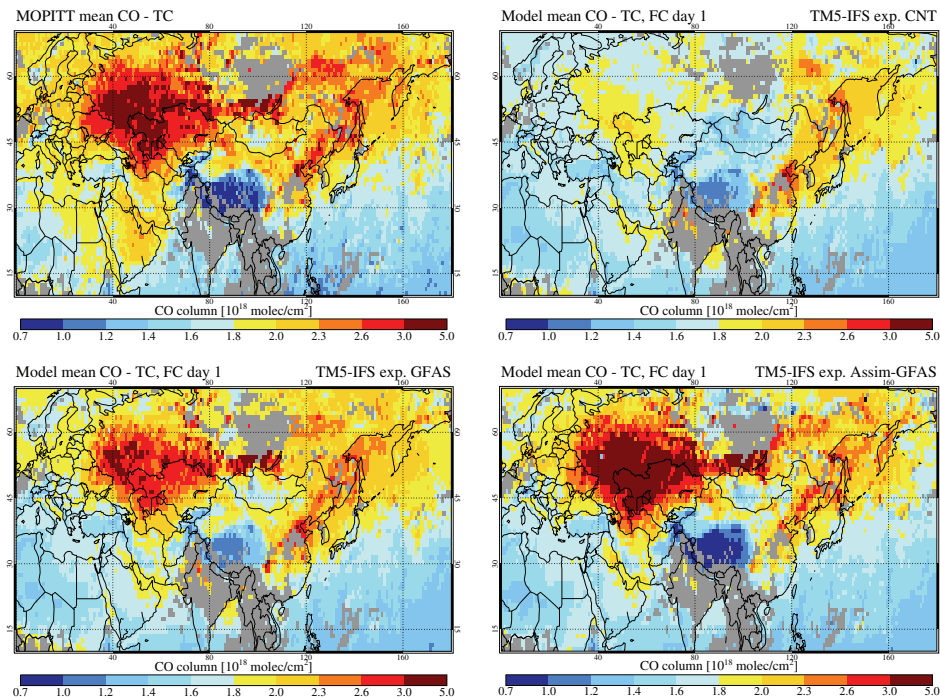


Fig. 5. Maps of mean CO columns from MOPITT-V4 for the time period 20 July–15 August 2010 compared to the kernel-weighted D + 0 CO columns from the runs CNT, GFAS and Assim-GFAS.

Title Page

Abstract	Introduction
Conclusions	References
Tables	Figures
◀	▶
◀	▶
Back	Close
Full Screen / Esc	
Printer-friendly Version	
Interactive Discussion	



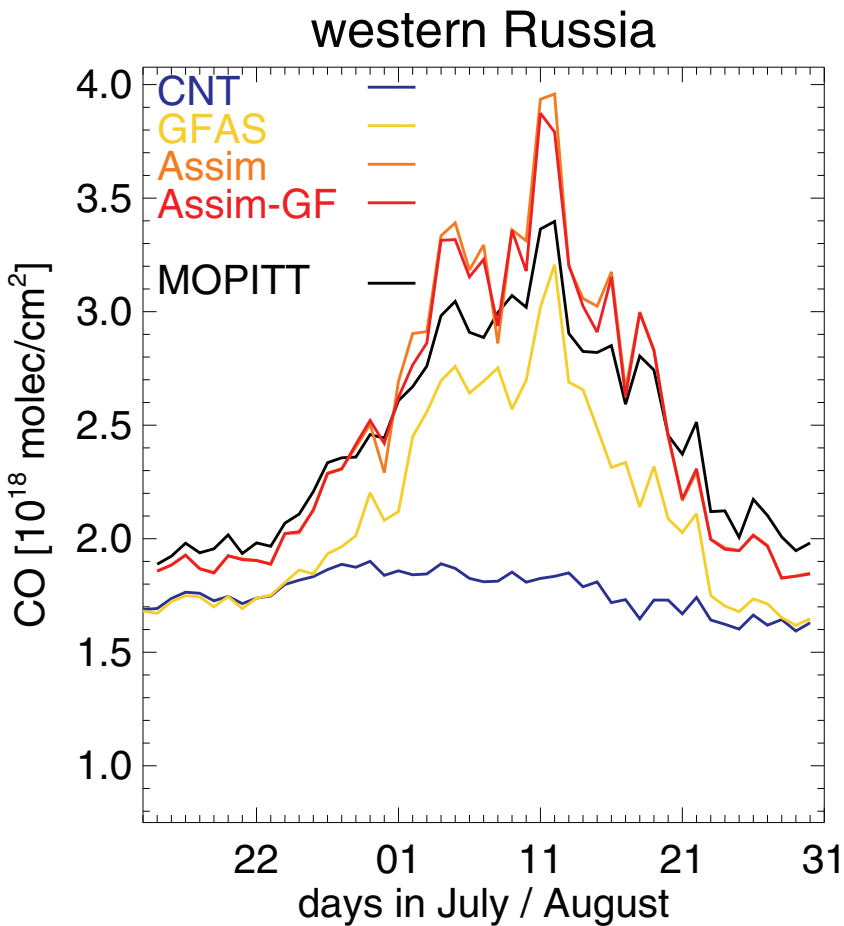


Fig. 6. Evolution of average kernel-weighted total columns over Western Russia compared to MOPITT, for D + 0 hindcasts.

Hindcast experiments of tropospheric composition

V. Huijnen et al.

Title Page

Abstract Introduction

Conclusions References

Tables Figures

⏪ ⏩

◀ ▶

Back Close

Full Screen / Esc

Printer-friendly Version

Interactive Discussion



Hindcast
experiments of
tropospheric
composition

V. Huijnen et al.

Title Page

Abstract

Introduction

Conclusions

References

Tables

Figures

◀

▶

◀

▶

Back

Close

Full Screen / Esc

Printer-friendly Version

Interactive Discussion

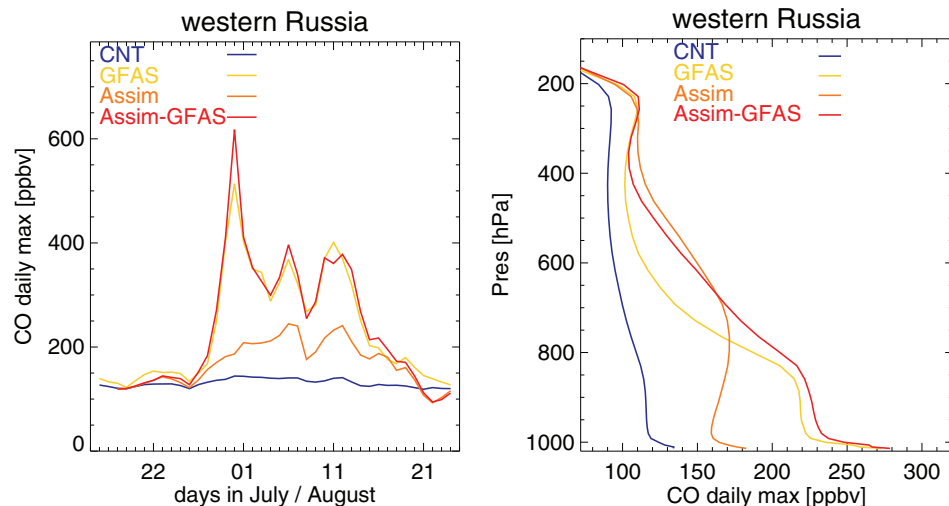


Fig. 7. (Left) maximum area-average surface CO concentrations for the four hindcast runs, at D + 0. (Right) averaged daily maximum CO profiles over Western Russia, for the time period 20 July–15 August.

Hindcast
experiments of
tropospheric
composition

V. Huijnen et al.

Title Page

Abstract

Introduction

Conclusions

References

Tables

Figures

◀

▶

◀

▶

Back

Close

Full Screen / Esc

Printer-friendly Version

Interactive Discussion

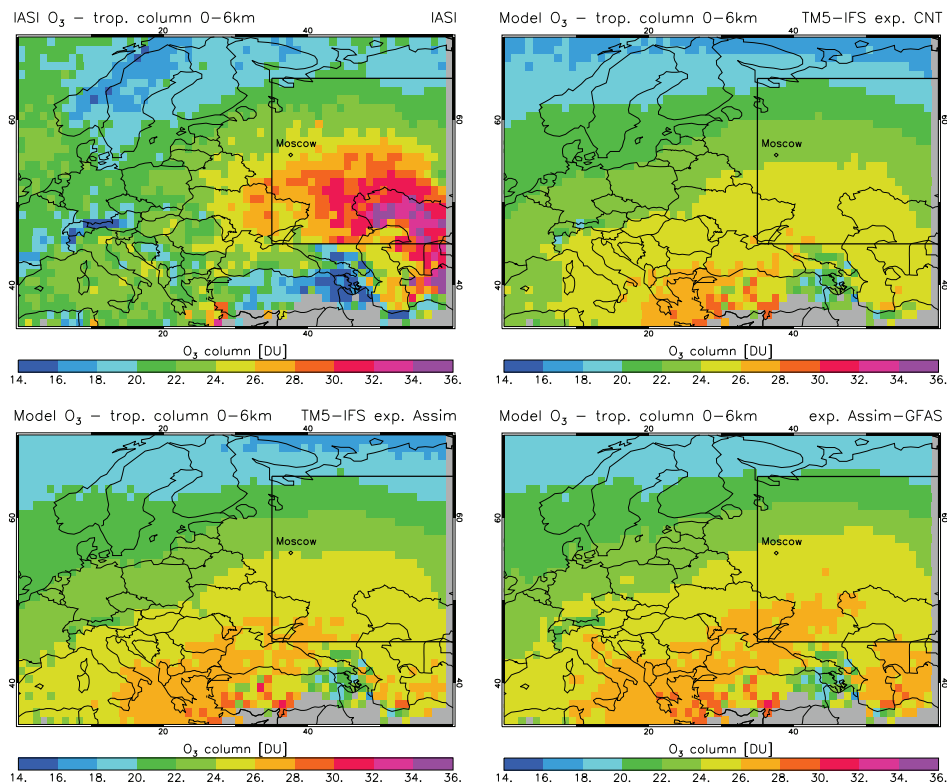


Fig. 8. Maps of mean O_3 tropospheric partial columns (0–6 km) as observed from IASI between 20 July and 15 August 2010 compared to the kernel-weighted D + 0 columns from the runs CNT, Assim and Assim-GFAS.

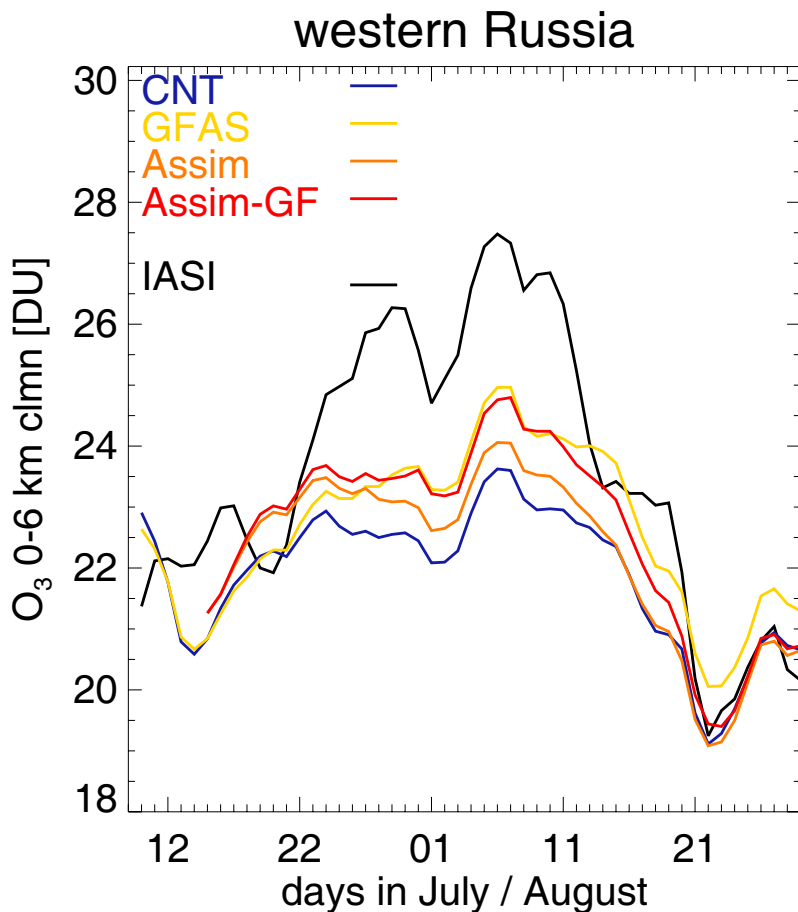


Fig. 9. Time series of modeled tropospheric O₃ columns (hindcast D + 0) with averaging kernel against IASI O₃ columns (0–6 km). Data are smoothed over a 3-day time window to filter out variations in spatial coverage.

**Hindcast
experiments of
tropospheric
composition**

V. Huijnen et al.

Title Page

Abstract

Introduction

Conclusions

References

Tables

Figures

◀

▶

◀

▶

Back

Close

Full Screen / Esc

Printer-friendly Version

Interactive Discussion

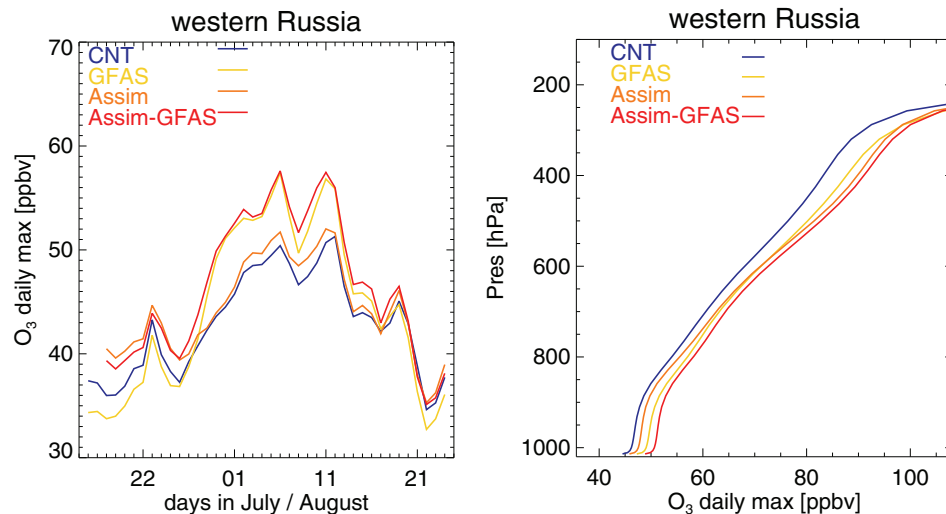


Fig. 10. (Left) maximum area-average surface O₃ concentrations over Western Russia for the four model settings, hindcast D + 0. (Right) corresponding time averaged profile of ozone daily maximum concentrations between 20 July and 15 August.

Hindcast experiments of tropospheric composition

V. Huijnen et al.

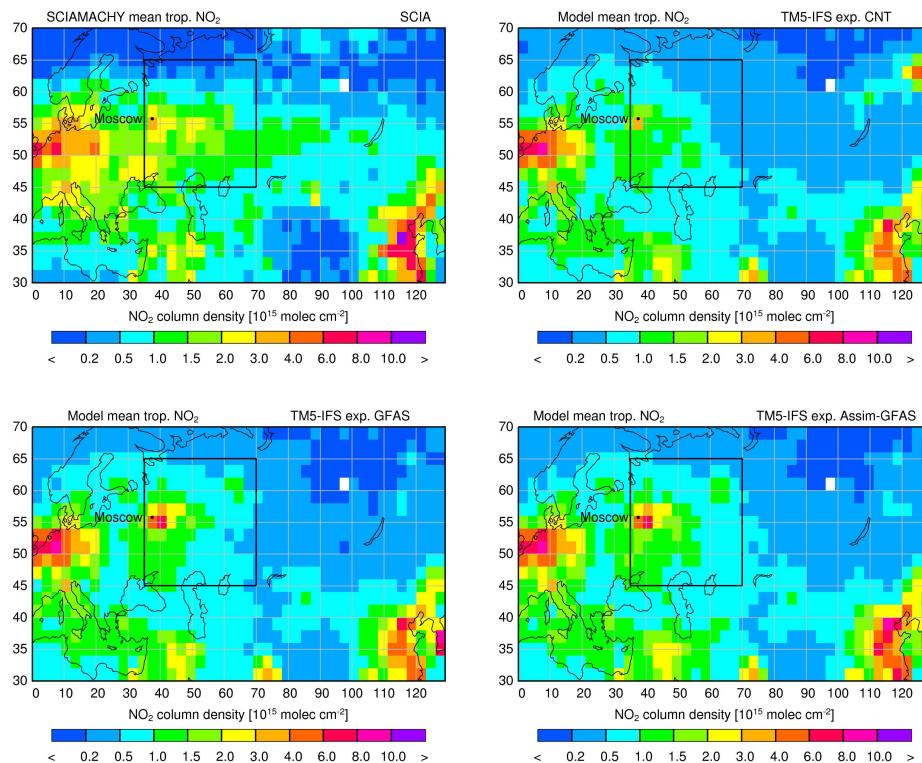


Fig. 11. Maps of mean tropospheric NO₂ columns as observed from SCIAMACHY between 20 July and 15 August compared to the D + 0 columns from the runs CNT, GFAS and Assim-GFAS.

Title Page

Abstract

Introduction

Conclusions

References

Tables

Figures

◀

▶

◀

▶

Back

Close

Full Screen / Esc

Printer-friendly Version

Interactive Discussion

**Hindcast
experiments of
tropospheric
composition**

V. Huijnen et al.

Title Page

Abstract

Introduction

Conclusions

References

Tables

Figures

◀

▶

◀

▶

Back

Close

Full Screen / Esc

Printer-friendly Version

Interactive Discussion

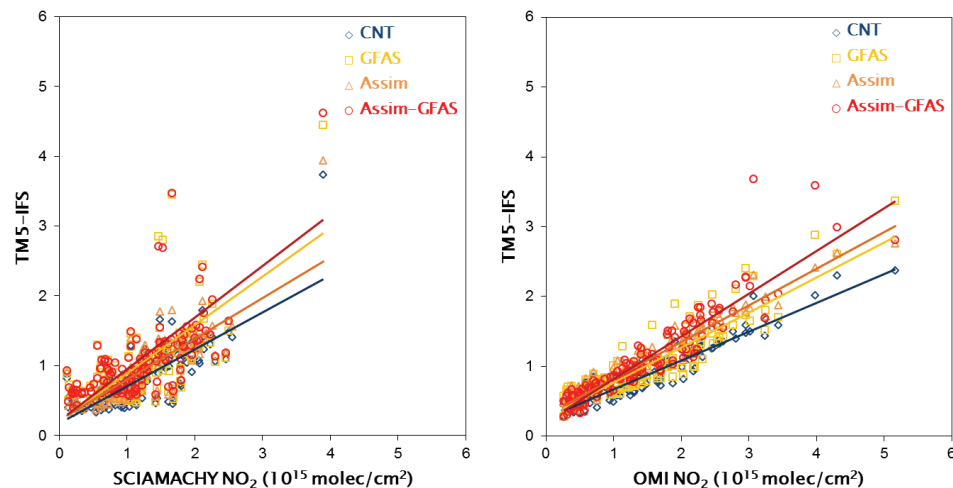


Fig. 12. Scatter plots of mean tropospheric NO₂ for model runs at D + 0 with respect to observations from SCIAMACHY and OMI, for the period 20 July to 15 August 2010.

Hindcast
experiments of
tropospheric
composition

V. Huijnen et al.

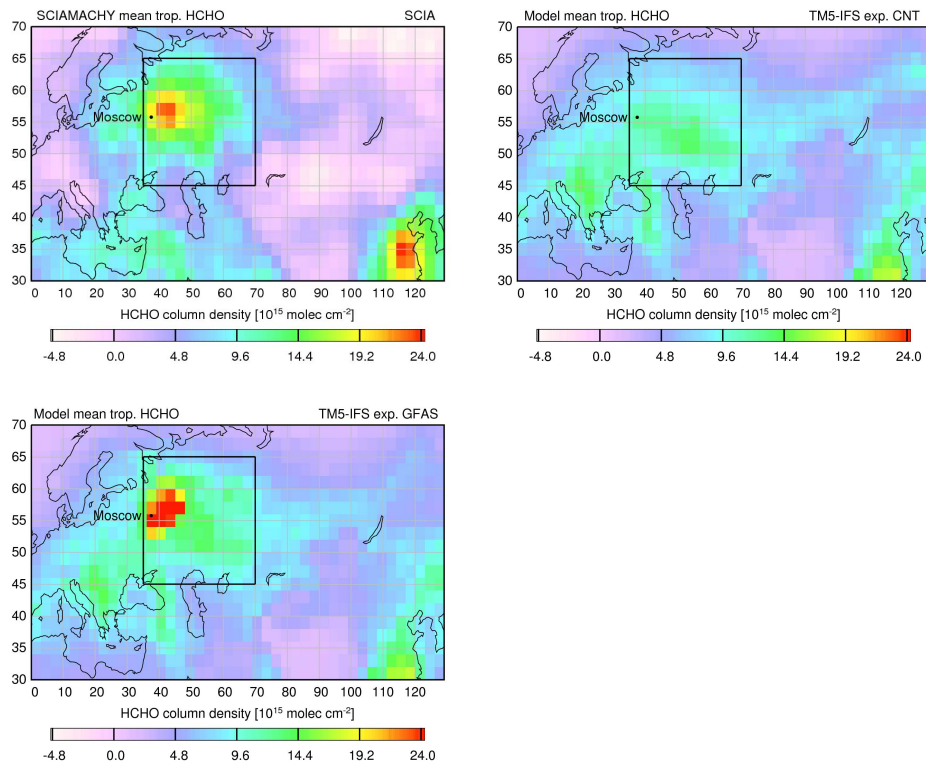


Fig. 13. Maps of mean tropospheric HCHO columns as observed from SCIAMACHY between 20 July and 15 August compared to the D + 0 columns from the runs CNT and GFAS.

Title Page

Abstract

Introduction

Conclusions

References

Tables

Figures

◀

▶

◀

▶

Back

Close

Full Screen / Esc

Printer-friendly Version

Interactive Discussion

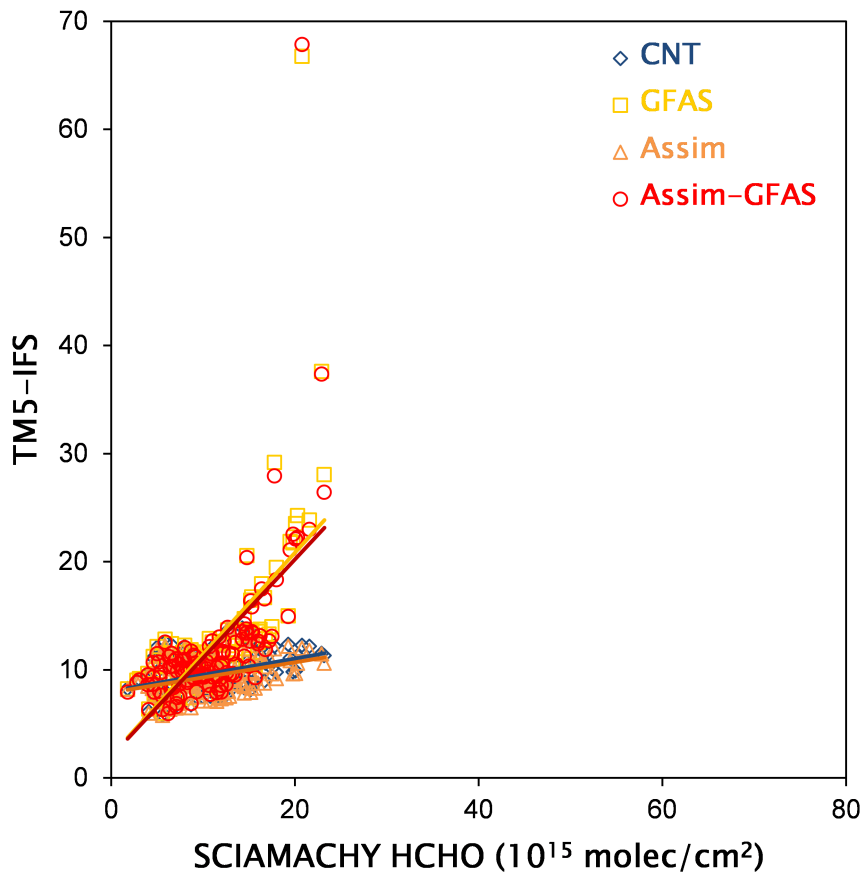


Fig. 14. Scatter plots of mean HCHO columns for model runs at D + 0 with respect to observations from SCIAMACHY, for the period 20 July to 15 August 2010.

Hindcast experiments of tropospheric composition

V. Huijnen et al.

Title Page

Abstract Introduction

Conclusions References

Tables Figures

⏪ ⏩

◀ ▶

Back Close

Full Screen / Esc

Printer-friendly Version

Interactive Discussion

